frontiers
in Applied Mathematics
and Statistics

TYPE Original Research
PUBLISHED 13 April 2026
DOI 10.3389/fams.2026.1799489

OPEN ACCESS

EDITED BY
Feng Rao,
Nanjing Tech University, China

REVIEWED BY
Parthasakha Das,
Rajiv Gandhi National Institute of Youth Development, India
Mohammed Moumni,
Moulay Ismail University, Morocco

*CORRESPONDENCE
Ifeanyi Sunday Onah
ifeanyi.onah@ndm.ox.ac.uk

RECEIVED 29 January 2026
REVISED 24 February 2026
ACCEPTED 02 March 2026
PUBLISHED 13 April 2026

CITATION
Asogwa CC and Onah IS (2026) A multi-host deterministic-stochastic framework for giardiasis transmission: branching-process extinction analysis and continuous-time Markov chain dynamics.
Front. Appl. Math. Stat. 12:1799489.
doi: 10.3389/fams.2026.1799489

A multi-host deterministic-stochastic framework for giardiasis transmission: branching-process extinction analysis and continuous-time Markov chain dynamics

Christopher Chukwuma Asogwa[1] and Ifeanyi Sunday Onah[1,2,3]*

[1]Department of Mathematics, University of Nigeria, Enugu, Nigeria, [2]Centre for Global Health Research, Nuffield Department of Medicine, University of Oxford, Oxford, United Kingdom, [3]Big Data Institute, Li Ka Shing Centre for Health Information and Discovery, University of Oxford, Oxford, United Kingdom

Giardiasis remains a widespread waterborne disease with substantial public health importance, particularly in settings with inadequate sanitation and high environmental contamination. In this study, we formulate and analyze a deterministic compartmental model that captures the transmission dynamics of *Giardia duodenalis* among immunocompetent and immunocompromised human populations, a lamb reservoir, and the environmental cyst pool. We derive the disease-free equilibrium and establish its local and global stability in terms of the basic reproduction number R_0, obtained via the next-generation matrix method. To complement the deterministic analysis, we construct a multi-type Galton-Watson branching process approximation near the DFE and compute type-specific extinction probabilities under different introduction scenarios. Sensitivity analysis is performed by varying key shedding parameters to quantify their influence on extinction likelihood. Furthermore, a continuous-time Markov chain (CTMC) model is developed to estimate the distribution of extinction times, providing additional insight into stochastic fadeout dynamics. Numerical experiments reveal that infections introduced through lambs or the environmental cyst reservoir exhibit markedly lower extinction probabilities and longer mean extinction times compared with human-initiated introductions. Overall, the combined deterministic-stochastic framework highlights the importance of reducing environmental contamination and targeting high-shedding hosts to enhance the probability of disease elimination. The results underscore the significance of early detection, timely treatment, and interventions that curtail environmental cyst persistence as effective strategies for mitigating giardiasis transmission.

KEYWORDS
branching process, CTMC extinction time, environmental transmission, giardiasis, multi-host epidemiological model, optimal control, sensitivity analysis

1 Introduction

Giardiasis is a globally prevalent intestinal infection caused by the protozoan *Giardia duodenalis* (also known as *G. lamblia or G. intestinalis*), a parasite capable of infecting humans and a wide range of domestic and wild animals [1, 2]. The World Health Organization classifies giardiasis among the neglected diseases associated with poverty and inadequate sanitation, with an estimated 280 million symptomatic cases annually, disproportionately affecting children under five years of age in low- and middle-income countries [3]. Transmission occurs primarily through the ingestion of environmentally persistent cysts, which may contaminate drinking water, food, soil, and fomites [4–6]. A single infected host can excrete up to 10^9 cysts per day, and the infectious dose can be as low as 10 cysts [7, 8], underscoring the extraordinary efficiency of its transmission.

From an epidemiological perspective, giardiasis is a zoonotic and environmentally mediated infection with transmission cycles influenced by human behavior, livestock management practices, and environmental conditions. Recent studies highlight the role of asymptomatic carriers, contaminated water systems, domestic animals, and environmental reservoirs in sustaining endemicity [9–12]. In agricultural settings, livestock, particularly young ruminants, may serve as amplifying hosts. The presence of viable cysts in pastureland and wastewater, therefore, complicates control efforts.

Mathematical modeling provides a crucial framework for understanding the persistence, control, and potential elimination of waterborne and environmentally transmitted pathogens. Previous deterministic models for giardiasis, such as those presented in Liana and Chuma [7], Edward and Shaban [8], and Das et al. [13, 14], have clarified the importance of direct and indirect transmission routes, environmental sanitation, and symptomatic/asymptomatic shedding. Similar modeling frameworks have been used for related protozoan infections, including cryptosporidiosis [15], where branching process theory and stochastic continuous-time Markov chain (CTMC) models have revealed that early stochastic fade-out can profoundly influence outbreak dynamics even when deterministic models predict persistence.

However, giardiasis is particularly sensitive to low-dose exposures and stochastic fluctuations, especially during the early stages of an outbreak when the number of infectious individuals is small. Deterministic formulations, while valuable for threshold analysis and long-term behavior, may overestimate persistence by smoothing out random extinction events and ignoring demographic stochasticity. Conversely, stochastic models, particularly multitype Galton-Watson branching processes and CTMC models, capture the probabilities of extinction, amplification, and outbreak variability [16, 17]. This interplay between deterministic and stochastic descriptions has recently become a key methodological theme in modern infectious disease modeling.

The present study develops a deterministic-stochastic modeling framework for giardiasis that incorporates immunocompetent humans, immunocompromised humans, lamb reservoirs, and environmental cyst concentrations. Immunocompromised individuals (I_m) often exhibit longer infectious periods and higher shedding intensity than immunocompetent individuals (I_c), and thus represent a distinct epidemiological subgroup of substantial importance. Lambs (I_l) serve as a major agricultural reservoir of zoonotic assemblages of Giardia, while the environmental compartment (G_p) captures cyst persistence and indirect transmission. This compartmental structure extends previous deterministic formulations [16] and aligns conceptually with the multi-host, multi-route transmission model used for cryptosporidiosis [15].

Using this structure, we derive the disease-free equilibrium, compute the basic reproduction number $\mathcal{R}_0$, and utilize next-generation methods to analyze local and global stability. To characterize extinction events and evaluate outbreak initiation across different host types, we formulate a four-type multitype branching process associated with the linearization of the deterministic model near the disease-free equilibrium. This approach parallels the stochastic methodology in, allowing precise computation of extinction probabilities P_0 for single-introduction scenarios. We further perform sensitivity analysis of the mean offspring matrix, highlighting how shedding rates ϕ_c, ϕ_m, ϕ_l influence outbreak fade-out under stochasticity. Full CTMC simulations are then used to approximate extinction-time distributions, an analysis crucial for understanding early outbreak kinetics and informing public health responses.

Overall, this study contributes to the giardiasis modeling literature by:

- Integrating deterministic, branching-process, and CTMC frameworks within a unified multi-host epidemiological model.
- Identifying transmission pathways and host types most likely to initiate sustained outbreaks, through analytically computed extinction probabilities.
- Evaluating the sensitivity of extinction dynamics to shedding parameters associated with humans and livestock.
- Estimating extinction time distributions, which provide operational insights into how rapidly outbreaks may fade without intervention.

The modeling results highlight how immunocompromised humans and lambs disproportionately drive persistence, whereas environmental-only introductions exhibit high extinction probability. These findings reinforce the need for targeted interventions in high-risk host groups and improved environmental sanitation strategies.

The remainder of this manuscript is organized as follows. Section 2 presents the deterministic model formulation, derives $\mathcal{R}_0$, equilibrium points, and stability conditions. Section 3 introduces the branching-process approximation and stochastic sensitivity analysis. Section 4 describes the CTMC simulations used to estimate extinction-time distributions. Finally, Section 5 summarizes the implications of our findings for giardiasis control and outlines directions for future research.

2 Deterministic model formulation

We consider a compartmental framework describing the transmission of giardiasis among human and lamb populations, together with an environmental reservoir of *Giardia* cysts. The total human population, denoted by N_h, and the total lamb population, denoted by N_l, are each stratified into epidemiological classes representing different stages of infection.

Specifically, individuals are classified as susceptible (S_j), exposed but not yet infectious (E_j), infectious and capable of transmitting the disease (I_j), or recovered with temporary or partial immunity (R_j). The subscript $j \in \{c, m, l\}$ identifies immunocompetent humans (c), immunocompromised humans (m), and lambs (l), respectively. In addition, G_p represents the concentration of viable *Giardia* cysts present in the environment.

Accordingly, the total population sizes are expressed as

$$N_h = N_c + N_m = S_c + E_c + I_c + R_c + S_m + E_m + I_m + R_m, 1 \tag{1}$$

$$N_l = S_l + E_l + I_l + R_l. \tag{2}$$

Susceptible immunocompromised humans acquire infection through effective contact with infectious humans, infectious lambs, or contaminated environmental cysts. The corresponding force of infection is given by

$$\lambda_m = \theta_c I_c + \theta_m I_m + \theta_l I_l + \theta_p G_p. \tag{3}$$

In contrast, susceptible immunocompetent humans experience a reduced infection risk, modeled as a proportional modification of λ_m, such that

$$\lambda_c = \epsilon_c \lambda_m. \tag{4}$$

Similarly, susceptible lambs become infected either through direct interaction with infectious lambs or via exposure to environmental cysts, with the force of infection given by

$$\lambda_l = \kappa_l I_l + \kappa_p G_p. \tag{5}$$

The parameters of the model are described in detail in Table 1. Therefore, following Figure 1 and given the description of the parameters as given in Equations 1–5 and the assumptions of the model, the deterministic model for the dynamics of giardiasis in humans and cattle is given below as

$$\begin{aligned}
\dot{S}_c &= \sigma_c \Lambda_h + \tau_c R_c - (\lambda_c + \mu_h + \beta_c) S_c, \\
\dot{E}_c &= \lambda_c S_c - (\mu_h + \eta_c) E_c, \\
\dot{I}_c &= \eta_c E_c - (\mu_h + d_c + r_c) I_c, \\
\dot{R}_c &= r_c I_c - (\mu_h + \tau_c) R_c, \\
\dot{S}_m &= (1 - \sigma_c) \Lambda_h + \tau_m R_m + \beta_c S_c - (\lambda_m + \mu_h) S_m, \\
\dot{E}_m &= \lambda_m S_m - (\mu_h + \eta_m) E_m, \\
\dot{I}_m &= \eta_m E_m - (\mu_h + d_m + r_m) I_m, \\
\dot{R}_m &= r_m I_m - (\mu_h + \tau_m) R_m, \\
\dot{S}_l &= \Lambda_l + \tau_l R_l - (\lambda_l + \mu_l) S_l, \\
\dot{E}_l &= \lambda_l S_l - (\mu_l + \eta_l) E_l, \\
\dot{I}_l &= \eta_l E_l - (\mu_l + d_l + r_l) I_l, \\
\dot{R}_l &= r_l I_l - (\mu_l + \tau_l) R_l, \\
\dot{G}_p &= \phi_c I_c + \phi_m I_m + \phi_l I_l - \mu_p G_p,
\end{aligned} \tag{6}$$

TABLE 1 Model parameters and their epidemiological interpretations.

Parameter	Meaning
σ_c	Fraction of newly recruited humans who are immunocompetent
Λ_h	Entry rate of individuals into the human population
τ_c	Waning rate of giardiasis-induced immunity among R_c
ε_c	Relative susceptibility reduction in immunocompetent humans S_c
θ_c	Transmission rate from infectious immunocompetent humans I_c to S_m
θ_m	Transmission rate from infectious immunocompromised humans I_m to S_m
θ_l	Transmission rate from infectious lambs I_l to S_m
θ_p	Environmental transmission rate from cysts G_p to S_m
$\varepsilon_c\theta_c$	Effective transmission rate from I_c to S_c
$\varepsilon_c\theta_m$	Effective transmission rate from I_m to S_c
$\varepsilon_c\theta_l$	Effective transmission rate from I_l to S_c
$\varepsilon_c\theta_p$	Effective transmission rate from environmental cysts to S_c
β_c	Rate at which immunocompetent humans lose immunity and enter S_m
μ_h	Baseline mortality rate in humans
η_c	Mean progression rate from exposed to infectious class E_c
η_m	Mean progression rate from exposed to infectious class E_m
d_c	Disease-induced mortality rate among I_c
d_m	Disease-induced mortality rate among I_m
r_c	Recovery rate of infectious immunocompetent humans
r_m	Recovery rate of infectious immunocompromised humans
ν_c	Rate of immunity loss in recovered immunocompetent humans R_c
ν_m	Rate of immunity loss in recovered immunocompromised humans R_m
Λ_l	Recruitment rate of lambs into the population
τ_l	Rate of immunity waning against giardiasis in R_l
κ_l	Direct transmission rate from infectious lambs I_l to S_l
κ_p	Environmental transmission rate from cysts G_p to S_l
μ_l	Natural mortality rate of lambs
η_l	Average latent-period progression rate in exposed lambs E_l
d_l	Giardiasis-related mortality rate in I_l
r_l	Recovery rate of infectious lambs
ϕ_c	Shedding rate of Giardia cysts into the environment by I_c
ϕ_m	Shedding rate of Giardia cysts into the environment by I_m
ϕ_l	Shedding rate of Giardia cysts into the environment by I_l
μ_p	Natural decay rate of Giardia cysts in the environment

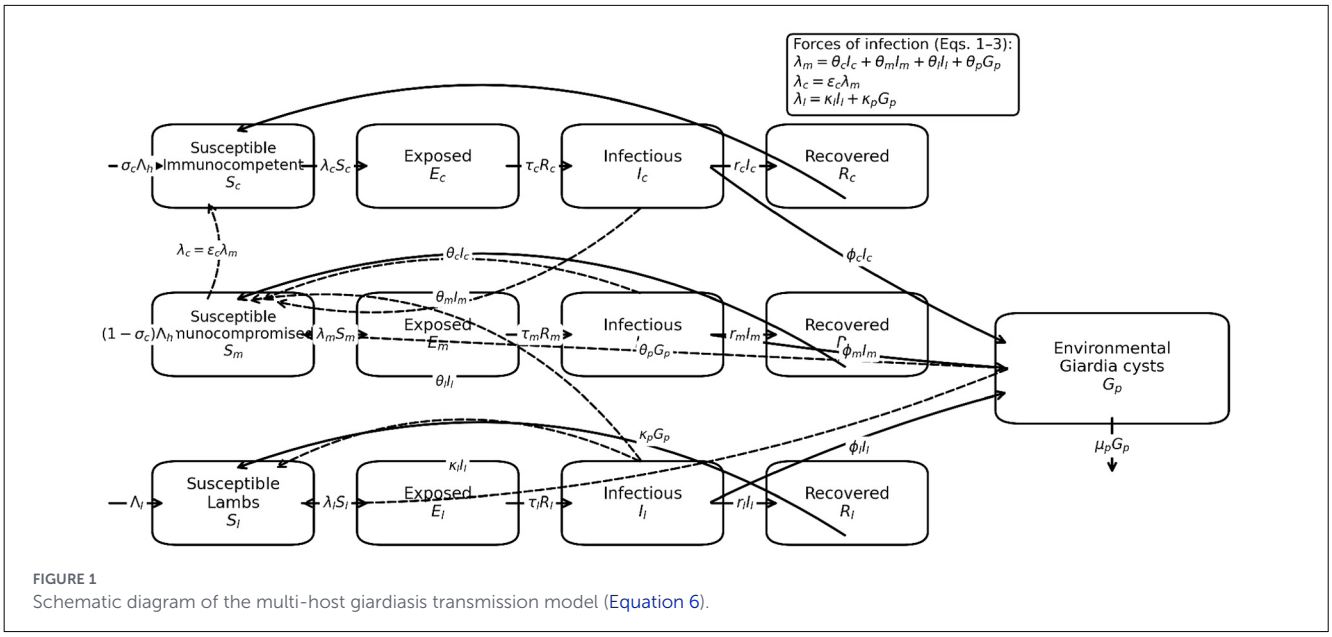

FIGURE 1
Schematic diagram of the multi-host giardiasis transmission model (Equation 6).

with initial non-negative conditions

$$S_c(0) > 0, \quad E_c(0) \geq 0, \quad I_c(0) \geq 0, \quad R_c(0) \geq 0, \quad S_m(0) > 0,$$
$$E_m(0) \geq 0, \quad I_m(0) \geq 0,$$
$$R_m(0) \geq 0, \quad S_l(0) > 0, \quad E_l(0) \geq 0, \quad I_l(0) \geq 0, \quad R_l(0) \geq 0,$$
$$\text{and} \quad G_p(0) \geq 0.$$

2.1 Qualitative analysis

This section establishes fundamental analytical properties of Equation 6. In particular, we demonstrate the positivity and boundedness of its solutions by invoking Lemma 2.1 and Theorem 2.1. We then derive conditions guaranteeing the existence of a unique endemic equilibrium via Theorem 2.3, and finally investigate the global asymptotic stability of the giardiasis disease-free equilibrium using Theorem 2.2.

2.1.1 Positivity of solutions and boundedness of Equation 6

We first verify the existence of solutions and show that all state variables remain non-negative for all future times.

Lemma 2.1. *Equation 6 possesses at least one solution. Furthermore, every solution originating in the region* $\Omega \subset \mathbb{R}^{13}_{+}$ *remains positive for all* $t \geq 0$.

Proof: To establish existence, uniqueness, and positivity of solutions, we first note that the right-hand side of Equation 6 consists of polynomial and bilinear incidence terms and is therefore continuously differentiable on $\mathbb{R}^{13}_{+}$. Hence, by the Picard–Lindelöf (Cauchy–Lipschitz) existence and uniqueness theorem [18, Theorem 3.1], there exists a unique local solution for any non-negative initial data. We now proceed to show that these solutions remain non-negative for all $t \geq 0$. To this end, we consider non-negative initial data and apply the integral operator $\int_0^t (\cdot)\, ds$ to each equation of Equation 6. For illustration, we examine the susceptible immunocompetent class,

$$\dot{S}_c = \sigma_c \Lambda_h + \tau_c R_c - (\lambda_c + \mu_h + \beta_c) S_c. \tag{7}$$

Integrating both sides of Equation 6 over the interval $[0, t]$ yields

$$\int_0^t \dot{S}_c\, ds = \int_0^t \left(\sigma_c \Lambda_h + \tau_c R_c - (\lambda_c + \mu_h + \beta_c) S_c\right) ds. \tag{8}$$

The left–hand side of Equation 7 simplifies to $S_c(t) - S_c(0)$, while the right–hand side can be decomposed as

$$\int_0^t \sigma_c \Lambda_h\, ds + \int_0^t \tau_c R_c(s)\, ds - \int_0^t (\lambda_c + \mu_h + \beta_c) S_c(s)\, ds. \tag{9}$$

Evaluating each integral term in Equation 7 gives

$$\int_0^t f(s)\, ds = \begin{cases} \sigma_c \Lambda_h\, t, & \text{if } f(s) = \sigma_c \Lambda_h, \\ \tau_c \int_0^t R_c(s)\, ds, & \text{if } f(s) = \tau_c R_c(s), \\ \int_0^t (\lambda_c + \mu_h + \beta_c) S_c(s)\, ds, & \text{if } f(s) = (\lambda_c + \mu_h + \beta_c) S_c(s), \end{cases} \tag{10}$$

which is standard for disease transmission dynamics.

Combining these expressions (*i.e.* Equations 7–10) leads to

$$S_c(t) = S_c(0) + \sigma_c \Lambda_h\, t + \tau_c \int_0^t R_c(s)\, ds - \int_0^t (\lambda_c + \mu_h + \beta_c) S_c(s)\, ds.$$

Since $S_c(0) \geq 0$, $\sigma_c \Lambda_h \geq 0$, and $R_c(s) \geq 0$ for all $s \in [0, t]$, it follows that all integral contributions are non–negative. Note that $(\lambda_c + \mu_h + \beta_c) S_c(s) \geq 0$ for all $s \geq 0$, since all parameters and

state variables are non–negative. Hence, the integral term $\int_0^t(\lambda_c + \mu_h + \beta_c)S_c(s)\,ds$ is non–negative, and Equation 10 provides a lower bound for $S_c(t)$. In particular, it follows that $S_c(t) \geq 0$ for all $t \geq 0$. Consequently,

$$\begin{aligned} S_c(t) \; &> S_c(0) + \sigma_c\Lambda_h\, t + \tau_c \int_0^t R_c(s)\,ds \\ &\quad - \int_0^t(\lambda_c + \mu_h + \beta_c)S_c(s)\,ds. \end{aligned} \tag{11}$$

Hence $S_c(t)$ remains positive for all $t \geq 0$.

Since $S_c(0) > 0$, $\sigma_c\Lambda_h > 0$, and $\tau_c R_c(s) \geq 0$ for all $s \in [0, t]$, it immediately follows that

$$S_c(t) > 0 \quad \text{for all } t \geq 0.$$

Next, we establish the positivity of the infectious immunocompetent class by examining

$$\dot{I}_c = \eta_c E_c - (\mu_h + d_c + r_c)I_c.$$

Rewriting Equation 11 and introducing the integrating factor $\mu(t) = e^{(\mu_h+d_c+r_c)t}$ yields

$$e^{(\mu_h+d_c+r_c)t}I_c = I_c(0) + \int_0^t \eta_c e^{(\mu_h+d_c+r_c)s}E_c(s)\,ds. \tag{12}$$

Solving explicitly for $I_c(t)$ gives

$$I_c(t) = e^{-(\mu_h+d_c+r_c)t}\left(I_c(0) + \int_0^t \eta_c e^{(\mu_h+d_c+r_c)s}E_c(s)\,ds\right).$$

Because $I_c(0) \geq 0$ and $E_c(s) \geq 0$ for all $s \geq 0$, we conclude that

$$I_c(t) \geq 0 \quad \text{for all } t \geq 0.$$

Using the same integrating-factor argument and noting that all inflow terms are non-negative whenever the state variables remain in $\mathbb{R}^{13}_+$, the positivity of the remaining compartments $E_c, R_c, S_m, E_m, I_m, R_m, S_l, E_l, I_l, R_l$, and G_p follows analogously.

By applying the same argument to the remaining compartments of Equation 6, we obtain

$$S_c(t) > 0,\; E_c(t) \geq 0,\; I_c(t) \geq 0,\; R_c(t) \geq 0,\; S_m(t) > 0,$$

$$E_m(t) \geq 0,\; I_m(t) \geq 0,\; R_m(t) \geq 0,$$

$$S_l(t) > 0,\; E_l(t) \geq 0,\; I_l(t) \geq 0,\; R_l(t) \geq 0,\; G_p(t) \geq 0, \quad \forall\, t \geq 0.$$

This completes the proof. □

Theorem 2.1. *All solutions of Equation 6 with initial conditions in* $\mathbb{R}^{13}_+$ *are uniformly bounded.*

Proof: We first divide Equation 6 into subsections of immunocompetent humans, immunocompromised humans, and lamb populations as follows:

For the immunocompetent humans, we have

$$\begin{aligned} &\tfrac{d(S_c+E_c+I_c+R_c)}{dt} \\ &= \sigma_c\Lambda_h + \tau_c R_c - (\lambda_c + \mu_h + \beta_c)S_c + \lambda_c S_c - (\mu_h + \eta_c)E_c + \eta_c E_c \\ &\quad -(\mu_h + d_c + r_c)I_c + r_c I_c - (\mu_h + \tau_c)R_c. \end{aligned}$$

□

Given that the total number of immunocompetent humans is given as $S_c + E_c + I_c + R_c = N_c$, then Equation 12 becomes

$$\frac{dN_c}{dt} = \sigma_c\Lambda_h - (S_c + E_c + I_c + R_c)\mu_h - \beta_c S_c - d_c I_c,$$

with $\beta_c, d_c \geq 0$,

$$\frac{dN_c}{dt} \leq \sigma_c\Lambda_h - \mu_h N_c.$$

Applying the standard comparison theorem for differential inequalities, we compare $N_c(t)$ with the solution of the linear auxiliary equation

$$\frac{dy}{dt} = \sigma_c\Lambda_h - \mu_h y, \qquad y(0) = N_c(0),$$

whose explicit solution is

$$y(t) = \frac{\sigma_c\Lambda_h}{\mu_h} + \left(N_c(0) - \frac{\sigma_c\Lambda_h}{\mu_h}\right)e^{-\mu_h t}.$$

Hence $N_c(t) \leq y(t)$ for all $t \geq 0$, which implies that $N_c(t)$ remains bounded. The same comparison argument applies to the remaining population components, thereby establishing the existence of a positively invariant bounded region Ω.

Solving this linear inequality with the integrating factor $e^{\mu_h t}$, we have

$$\frac{d}{dt}\left(e^{\mu_h t}N_c(t)\right) \leq \sigma_c\Lambda_h e^{\mu_h t}.$$

Integrating from 0 to t gives

$$e^{\mu_h t}N_c(t) - N_c(0) \leq \frac{\sigma_c\Lambda_h}{\mu_h}(e^{\mu_h t} - 1).$$

Hence,

$$N_c(t) \leq \frac{\sigma_c\Lambda_h}{\mu_h} + \left(N_c(0) - \frac{\sigma_c\Lambda_h}{\mu_h}\right)e^{-\mu_h t}.$$

As $t \to \infty$,

$$N_c(t) \leq \frac{\sigma_c\Lambda_h}{\mu_h},$$

so the positively invariant region is

$$\begin{aligned} \Omega_c \; &= \{(S_c, E_c, I_c, R_c) \in \mathbb{R}^4_+ : 0 \leq S_c + E_c + I_c + R_c \\ &\qquad \leq \sigma_c\Lambda_h/\mu_h. \end{aligned}$$

So, using the same procedure, it can be concluded that

$$\begin{aligned} \Omega_m \; &= \{(S_m, E_m, I_m, R_m) \in \mathbb{R}^4_+ : 0 \leq S_m + E_m + I_m + R_m \\ &\leq (1 - \sigma_c)\Lambda_h/\mu_h\}, \\ \Omega_l \; &= \{(S_l, E_l, I_l, R_l) \in \mathbb{R}^4_+ : 0 \leq S_l + E_l + I_l + R_l \leq \Lambda_l/\mu_l\}, \\ M(t) \leq \Omega_p \; &= \max\left\{\frac{\sigma_c\Lambda_h\phi_c}{\mu_h\mu_p} + \frac{((1-\sigma_c)\Lambda_h\phi_m)}{\mu_h\mu_p} + \frac{\Lambda_l\phi_l}{\mu_l\mu_p}, G_P(0)\right\}, \end{aligned}$$

Thus, all trajectories of the model remain biologically feasible and mathematically well-defined, and every solution of Equation 6 evolves within the positively invariant region Ω.

2.2 Equilibrium points of Equation 4

2.2.1 Giardiasis disease-free equilibrium point E^0

When giardiasis is absent from the lamb population, as well as from both immunocompetent individuals and immunocompromised human subgroups, Equation 6 admits a disease–free steady state given by

$$E^0 = \left(\frac{\sigma_c\Lambda_h}{k_1}, 0, 0, 0, \frac{k_2\Lambda_h}{\mu_h k_1}, 0, 0, 0, \frac{\Lambda_l}{\mu_l}, 0, 0, 0, 0\right), \quad (13)$$

where $k_1 = \mu_h + \beta_c$ and $k_2 = \beta_c + \mu_h(1-\sigma_c)$.

2.2.2 Basic reproduction number $\mathcal{R}_0$

The basic reproduction number $\mathcal{R}_0$ quantifies the expected number of secondary infections generated by a single infectious individual introduced into a fully susceptible population over its infectious lifetime [19]. Employing the next–generation matrix methodology [20], the threshold parameter associated with Equation 6 is obtained as

$$\mathcal{R}_0 = \frac{1}{2}\left(\mathcal{R}_{hp} + \mathcal{R}_{lp} + \sqrt{(\mathcal{R}_{hp} - \mathcal{R}_{lp})^2 + 4\mathcal{R}_{lhp}}\right).$$

Here,

$$\mathcal{R}_{hp} = \frac{\left(k_5k_6\mu_h\eta_c\sigma_c(\mu_p\theta_c + \phi_c\theta_p) + k_2k_3k_4\eta_m(\mu_p\theta_m + \phi_m\theta_p)\right)\Lambda_h}{k_1k_3k_4k_5k_6\mu_h\mu_p},$$

$$\mathcal{R}_{lp} = \frac{(\kappa_l\mu_p + \kappa_p\phi_l)\eta_l\Lambda_l}{k_7k_8\mu_l\mu_p},$$

$$\mathcal{R}_{lhp} = \frac{\left(k_5k_6\mu_h\varepsilon_c\eta_c\sigma_c\phi_c + k_2k_3k_4\eta_m\phi_m\right)(\mu_p\theta_l + \phi_l\theta_p)\eta_l\kappa_p\Lambda_l\Lambda_h}{k_1k_3k_4k_5k_6k_7k_8\mu_h\mu_p^2}.$$

The constants are defined as $k_1 = \mu_h+\beta_c$, $k_2 = \beta_c+(1-\sigma_c)\mu_h$, $k_3 = \mu_h+\eta_c$, $k_4 = d_c+r_c+\mu_h$, $k_5 = \mu_h+\eta_m$, $k_6 = \mu_h+d_m+r_m$, $k_7 = \mu_l+\eta_l$, and $k_8 = \mu_l+d_l+r_l$. The quantities $\mathcal{R}_{hp}$, $\mathcal{R}_{lp}$, and $\mathcal{R}_{lhp}$ represent the partial reproduction numbers associated with transmission involving humans and the environment, lambs and the environment, and their combined interaction, respectively.

2.2.3 Giardiasis persistent equilibrium point E^*

The equilibrium point E^* corresponds to a steady state in which giardiasis coexists within immunocompetent humans, immunocompromised humans, and the lamb population. This equilibrium is obtained by equating the right-hand sides of Equation 6 to zero and solving the resulting nonlinear algebraic system simultaneously. The endemic equilibrium is expressed as

$$E^* = \left(S_c^*, E_c^*, I_c^*, R_c^*, S_m^*, E_m^*, I_m^*, R_m^*, S_l^*, E_l^*, I_l^*, R_l^*\right),$$

in terms of λ_m^* where

$$R_c^* = \frac{r_cI_c^*}{k_{10}}, \quad S_c^* = \frac{k_{10}\sigma_c\Lambda_h + r_c\tau_cI_c^*}{k_{10}(\epsilon_c\lambda_m^* + k_1)},$$

$$E_c^* = \frac{\epsilon\lambda_m^*(k_{10}\sigma_c\Lambda_h + r_c\tau_cI_c^*)}{k_3k_{10}(\epsilon_c\lambda_m^* + k_1)}, \quad R_m^* = \frac{r_mI_m^*}{k_{12}},$$

$$I_c^* = \frac{k_{10}\epsilon_c\eta_c\sigma_c\Lambda_h\lambda_m^*}{(k_3k_4k_{10} - \eta_cr_c\tau_c)\epsilon_c\lambda_m^* + k_3k_4k_{10}k_1},$$

$$E_m^* = \frac{\lambda_m^*S_m^*}{k_5}, \quad I_m^* = \frac{\eta_mE_m^*}{k_6}, \quad E_l^* = \frac{k_8I_l^*}{\eta_l},$$

$$S_m^* = \frac{(1-\sigma_c)\Lambda_h + \beta_cS_c^* + \tau_mR_m^*}{(\lambda_m^* + \mu_h)},$$

$$G_p^* = \frac{\phi_cI_c^* + \phi_mI_m^* + \phi_lI_l^*}{\mu_p}, \quad R_l^* = \frac{r_lI_l^*}{k_7},$$

$$I_l^* = \frac{\lambda_m^* - (\theta_cI_c^* + \theta_mI_m^* + \theta_pG_p^*)}{\theta_l},$$

$$\lambda_l^* = \rho_lI_l^* + \rho_pG_p^*, \quad S_l^* = \frac{k_7E_l^*}{\lambda_l^*}.$$

Substituting S_l^*, R_l^*, and λ_l^* into the susceptible-lamb equation of Equation 6 and evaluating it at the endemic equilibrium yields a polynomial equation of degree five in λ_m^* of the form

$$c_5(\lambda_m^*)^5 + c_4(\lambda_m^*)^4 + c_3(\lambda_m^*)^3 + c_2(\lambda_m^*)^2 + c_1\lambda_m^* + c_0 = 0. \quad (14)$$

The coefficients $c_5, \ldots, c_0$ depend explicitly on the parameters of the model. In particular, the leading and constant coefficients are given by

$$\begin{aligned} c_0 &= k_2^2k_3^2k_4^2k_{10}^2k_5k_6k_{12}k_7k_8k_{14}k_1k_{15}\mu_h\mu_l\mu_p\eta_l \\ &\quad \times \left(1 + R_0 - (R_{hp} + R_{lp})\right)(1 - R_0), \\ c_5 &= \varepsilon_c^2\eta_l\mu_p(\phi_l\rho_p + \rho_l\mu_p)(k_7k_4k_{10} - \eta_cr_c\tau_c)^2 \\ &\quad \times (k_5k_6k_{12} - \eta_mr_m\tau_m)^2(k_7k_8k_{14} - \eta_lr_l\tau_l), \end{aligned}$$

where $k_9 = \lambda_c + \beta_c + \mu_h$, $k_{10} = \tau_c + \mu_h$, $k_{11} = \lambda_m + \mu_h$, $k_{12} = \tau_m + \mu_h$, $k_{13} = \lambda_l + \mu_l$, $k_{14} = \tau_l + \mu_l$, and $k_{15} = \phi_l\theta_p + \mu_p\theta_l$.

To establish the existence of a unique persistent equilibrium, note that $(k_7k_8k_{14} - \eta_lr_l\tau_l) = \mu_l(d_l+\mu_l+r_l)(\mu_l+\eta_l+\tau_l) + \eta_l\tau_l(d_l+\mu_l) > 0$, which implies $c_5 > 0$. Moreover, if $1 + R_0 > (R_{hp} + R_{lp})$, then $c_0 < 0$ for $R_0 > 1$ and $c_0 > 0$ for $R_0 < 1$.

Consequently, when $\mathcal{R}_0 > 1$, the sequence of coefficients $(c_5, \ldots, c_0)$ exhibits at least one sign change. By Descartes' rule of signs, Equation 14 therefore admits at least one positive real root whenever $\mathcal{R}_0 > 1$, ensuring the existence of a persistent equilibrium. Depending on parameter values, Equation 14 may also admit no positive solution or multiple positive solutions, corresponding to the absence or multiplicity of endemic equilibria. The stability properties of these equilibrium states are investigated in subsequent sections.

2.3 Stability analysis of equilibrium states

2.3.1 Global stability of giardiasis disease-free equilibrium point E^0

Given the giardiasis disease-free equilibrium point E^0 given in Equation 13, we show below that E^0 is globally asymptotically stable when $\mathcal{R}_0 < 1$.

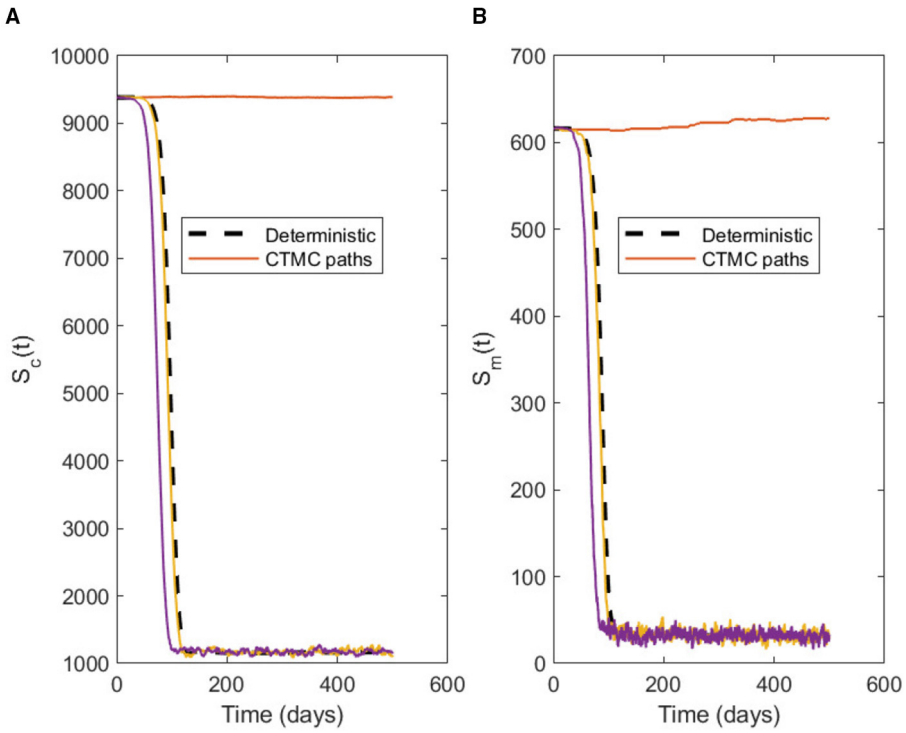

FIGURE 2
Representative realizations of the CTMC-based stochastic dynamics (solid curves) compared with the associated deterministic trajectories (dashed curves) for **(A)** the susceptible immunocompetent human population S_c and **(B)** the susceptible immunocompromised human population S_m. Solid curves represent multiple stochastic realizations of the CTMC model, included to illustrate demographic randomness and variability in outbreak trajectories, while dashed curves denote the corresponding deterministic solution.

Theorem 2.2. *The giardiasis disease-free equilibrium point E^0 is globally asymptotically stable when $\mathcal{R}_0 < 1$ and unstable otherwise.*

Proof: We prove the global stability of the DFE point E^0 of the giardiasis model (Equation 6) by adopting the Metzler matrix approach described by Kamgang and Sallet [21]. To do this, we write the model Equation 6 as

$$\begin{cases} \frac{dU_s}{dt} = A_0(U_s - U(E^0)) + A_1 U_i, \\ \frac{dU_i}{dt} = A_2 U_i, \end{cases}$$

where U_s is the vector denoting the compartments in our system that do not transmit the giardiasis disease, and U_i denotes the giardiasis-transmitting vector components. Here, if A_2 is a Metzler matrix (*i.e.*, the off-diagonal entries of A_2 are non-negative), and A_0 has real negative eigenvalues, then the giardiasis-free equilibrium is globally asymptotically stable. Now, from the model Equation 6, we have $U_s = (S_c, R_c, S_m, R_m, S_l, R_l)^T$, $U_i = (E_c, I_c, E_m, I_m, E_l, I_l, G_p)^T$ and

$$U_s - U(E^0) = \begin{pmatrix} S_c - \frac{\sigma_c \Lambda_h}{k_1} \\ R_c \\ S_m - \frac{k_2 \Lambda_h}{\mu_h k_1} \\ R_m \\ S_l - \frac{\Lambda_l}{\mu_l} \\ R_l \end{pmatrix},$$

$$A_0 = \begin{pmatrix} -(\mu_h + \beta_c) & \tau_c & 0 & 0 & 0 & 0 \\ 0 & -(\mu_h + \tau_c) & 0 & 0 & 0 & 0 \\ \beta_c & 0 & -\mu_h & \tau_m & 0 & 0 \\ 0 & 0 & 0 & -(\mu_h + \tau_m) & 0 & 0 \\ 0 & 0 & 0 & 0 & -\mu_l & \tau_l \\ 0 & 0 & 0 & 0 & 0 & -(\mu_l + \tau_l) \end{pmatrix}.$$

The eigenvalues of the matrix A_0 are $\lambda_1 = -\mu_h$, $\lambda_2 = -(\mu_h + \tau_c)$, $\lambda_3 = -(\mu_h + \beta_c)$, $\lambda_4 = -(\mu_h + \tau_m)$, $\lambda = -\mu_l$ and $\lambda_6 = -(\mu_l + \tau_l)$. Also we have

$$A_1 = \begin{pmatrix} 0 & \frac{\epsilon_c \theta_c \sigma_c \Lambda_h}{k_1} & 0 & \frac{\epsilon_c \theta_m \sigma_c \Lambda_h}{k_1} & 0 & \frac{\epsilon_c \theta_l \sigma_c \Lambda_h}{k_1} & \frac{\epsilon_c \theta_p \sigma_c \Lambda_h}{k_1} \\ 0 & r_c & 0 & 0 & 0 & 0 & 0 \\ 0 & \frac{\theta_c k_2 \Lambda_h}{\mu_h k_1} & 0 & \frac{\theta_m k_2 \Lambda_h}{\mu_h k_1} & 0 & \frac{\theta_l k_2 \Lambda_h}{\mu_h k_1} & \frac{\theta_p k_2 \Lambda_h}{\mu_h k_1} \\ 0 & 0 & 0 & r_m & 0 & 0 & 0 \\ 0 & 0 & 0 & 0 & 0 & \frac{\kappa_l \Lambda_l}{\mu_l} & \frac{\kappa_p \Lambda_l}{\mu_l} \\ 0 & 0 & 0 & 0 & 0 & r_l & 0 \end{pmatrix},$$

$$A_2 = \begin{pmatrix} -(\mu_h + \eta_c) & \frac{\epsilon_c \theta_c \sigma_c \Lambda_h}{k_1} & 0 & \frac{\epsilon_c \theta_m \sigma_c \Lambda_h}{k_1} & 0 & \frac{\epsilon_c \theta_l \sigma_c \Lambda_h}{k_1} & \frac{\epsilon_c \theta_p \sigma_c \Lambda_h}{k_1} \\ \tau_c & -(\mu_h + d_c + r_c) & 0 & 0 & 0 & 0 & 0 \\ 0 & \frac{\theta_c k_2 \Lambda_h}{\mu_h k_1} & -(\mu_h + \eta_m) & \frac{\theta_m k_2 \Lambda_h}{\mu_h k_1} & 0 & \frac{\theta_l k_2 \Lambda_h}{\mu_h k_1} & \frac{\theta_p k_2 \Lambda_h}{\mu_h k_1} \\ 0 & 0 & \eta_m & -(\mu_h + d_m + r_m) & 0 & 0 & 0 \\ 0 & 0 & 0 & 0 & -(\mu_l + \eta_l) & \frac{\kappa_l \Lambda_l}{\mu_l} & \frac{\kappa_k \Lambda_l}{\mu_l} \\ 0 & \phi_c & 0 & \phi_m & 0 & \phi_l & -\mu_p \end{pmatrix}.$$

Given that the eigenvalues of the matrix A_0 are negative and the off-diagonal entries of the Metzler matrix If A_2 are non-negative, it follows that the giardiasis disease-free equilibrium point E^0 is globally asymptotically stable.

The transient "overshoot" observed in Figure 2, where human infections initially exceed their long-term endemic level before

stabilizing, has important biological implications. This behavior reflects rapid epidemic growth when the population is largely susceptible and environmental cyst concentrations accumulate faster than removal processes. During the early phase, high shedding rates temporarily amplify transmission, producing a peak in infections before feedback mechanisms, including recovery, waning susceptibility, and environmental cyst decay, reduce the effective force of infection. Such overshoot dynamics are characteristic of environmentally mediated diseases and suggest that short-term case surges may occur even when the system ultimately converges to a stable endemic equilibrium. From a public-health perspective, this highlights the importance of early intervention and environmental sanitation to mitigate peak healthcare burden during outbreak initiation. □

2.3.2 Global stability of giardiasis persistent equilibrium E^*

Here, we analyze the global stability of the persistent equilibrium of our model Equation 6 by stating and proving the following theorem.

Theorem 2.3. *The unique persistent equilibrium E^* is globally asymptotically stable if $\mathcal{R}_0 > 1$ and unstable otherwise.*

Proof: We first define the Lyapunov function

$$\begin{aligned}\mathscr{L} &= \kappa_1\left(S_c - S_c^* - S_c^*\ln\frac{S_c}{S_c^*}\right) + \kappa_2\left(E_c - E_c^* - E_c^*\ln\frac{E_c}{E_c^*}\right)\\ &+ \kappa_3\left(I_c - I_c^* - I_c^*\ln\frac{I_c}{I_c^*}\right)\\ &+ \kappa_4\left(R_c - R_c^* - R_c^*\ln\frac{R_c}{R_c^*}\right) + \kappa_5\left(S_m - S_m^* - S_m^*\ln\frac{S_m}{S_m^*}\right)\\ &+ \kappa_6\left(E_m - E_m^* - E_m^*\ln\frac{E_m}{E_m^*}\right)\\ &+ \kappa_7\left(I_m - I_m^* - I_m^*\ln\frac{I_m}{I_m^*}\right) + \kappa_8\left(R_m - R_m^* - R_m^*\ln\frac{R_m}{R_m^*}\right)\\ &+ \kappa_9\left(S_l - S_l^* - S_l^*\ln\frac{S_l}{S_l^*}\right)\\ &+ \kappa_{10}\left(E_l - E_l^* - E_l^*\ln\frac{E_l}{E_l^*}\right) + \kappa_{11}\left(I_l - I_l^* - I_l^*\ln\frac{I_l}{I_l^*}\right)\\ &+ \kappa_{12}\left(R_l - R_l^* - R_l^*\ln\frac{R_l}{R_l^*}\right)\\ &+ \kappa_{13}\left(G_p - G_p^* - G_p^*\ln\frac{G_p}{G_p^*}\right),\end{aligned}$$

following the definition by Mgandu et al. [22] and Stephano et al. [23]. The time derivative of the Lyapunov function $\mathscr{L}$ is given below as

$$\begin{aligned}\frac{d\mathscr{L}}{dt} &= \kappa_1\left(1-\frac{S_c^*}{S_c}\right)\frac{dS_c}{dt} + \kappa_2\left(1-\frac{E_c^*}{E_c}\right)\frac{dE_c}{dt}\\ &+ \kappa_3\left(1-\frac{I_c^*}{I_c}\right)\frac{dI_c}{dt} + \kappa_4\left(1-\frac{R_c^*}{R_c}\right)\frac{dR_c}{dt}\\ &+ \kappa_5\left(1-\frac{S_m^*}{S_m}\right)\frac{dS_m}{dt} + \kappa_6\left(1-\frac{E_m^*}{E_m}\right)\frac{dE_m}{dt}\\ &+ \kappa_7\left(1-\frac{I_m^*}{I_m}\right)\frac{dI_m}{dt} + \kappa_8\left(1-\frac{R_m^*}{R_m}\right)\frac{dR_m}{dt}\\ &+ \kappa_9\left(1-\frac{S_l^*}{S_l}\right)\frac{dS_l}{dt} + \kappa_{10}\left(1-\frac{E_l^*}{E_l}\right)\frac{dE_l}{dt}\\ &+ \kappa_{11}\left(1-\frac{I_l^*}{I_l}\right)\frac{dI_l}{dt} + \kappa_{12}\left(1-\frac{R_l^*}{R_l}\right)\frac{dR_l}{dt}\\ &+ \kappa_{13}\left(1-\frac{G_p^*}{G_p}\right)\frac{dG_p}{dt}. \qquad (15)\end{aligned}$$

Let

$$\begin{aligned}&a = \frac{\lambda_m}{\lambda_m^*},\quad b = \frac{S_c}{S_c^*},\quad d = \frac{E_c}{E_c^*},\quad e = \frac{I_c}{I_c^*},\quad f = \frac{R_c}{R_c^*},\quad g = \frac{S_m}{S_m^*},\\ &h = \frac{E_m}{E_m^*},\quad m = \frac{I_m}{I_m^*},\quad n = \frac{R_m}{R_m^*},\\ &p = \frac{\lambda_l}{\lambda_l^*},\quad q = \frac{S_l}{S_l^*},\quad u = \frac{E_l}{E_l^*},\quad x = \frac{I_l}{I_l^*},\quad y = \frac{R_l}{R_l^*},\quad z = \frac{G_p}{G_p^*}.\end{aligned}$$

Substituting the equations of model Equation 6 into Equation 15 at steady state gives

$$\begin{aligned}&\tfrac{d\mathscr{L}}{dt}\\ &= -\kappa_1 k_1 S_c\left(1-\frac{1}{b}\right)^2 - \kappa_5\mu_h S_m\left(1-\frac{1}{g}\right)^2 - \kappa_9\mu_l S_l\left(1-\frac{1}{q}\right)^2\\ &+ \kappa_1\left(1-\frac{1}{b}\right)(\tau_c R_c^*(f-1) + \epsilon_c\lambda_m^* S_c^*(1-ab))\\ &+ \kappa_2\epsilon_c\lambda_m^* S_c^*\left(1-\frac{1}{d}\right)(ab-d)\\ &+ \kappa_3\eta_c E_c^*\left(1-\frac{1}{e}\right)(d-e) + \kappa_4 r_c I_c^*\left(1-\frac{1}{f}\right)(e-f)\\ &+ \kappa_5\left(1-\frac{1}{g}\right)(\beta_c S_c^*(b-1) + \tau_m R_m^*(n-1)\\ &+ \lambda_m^* S_m^*(1-ag)) + \kappa_6\lambda_m^* S_m^*\left(1-\frac{1}{h}\right)(ag-h)\\ &+ \kappa_7\eta_m E_m^*\left(1-\frac{1}{m}\right)(h-m) + \kappa_8 r_m I_m^*\left(1-\frac{1}{n}\right)(m-n)\\ &+ \kappa_9\left(1-\frac{1}{q}\right)(\tau_l R_l^*(y-1) + \lambda_l^* S_l^*(1-pq))\\ &+ \kappa_{10}\lambda_l^* S_l^*\left(1-\frac{1}{u}\right)(pq-u)\\ &+ \kappa_{11}\eta_l E_l^*\left(1-\frac{1}{x}\right)(u-x) + k_{12} r_l I_l^*\left(1-\frac{1}{y}\right)(x-y)\\ &+ \kappa_{13}\left(1-\frac{1}{z}\right)(\phi_c I_c^*(e-z) + \phi_m I_m^*(m-z)) \qquad (16)\\ &+ \kappa_{13}\phi_l I_l^*\left(1-\frac{1}{z}\right)(x-z).\end{aligned}$$

Simplifying further and setting the coefficients of ab, ag, d, f, h, n, pq, u, and y to zero, we have

$$\begin{aligned}&\kappa_1 = \kappa_2 = \kappa_5 = \kappa_6 = \kappa_9 = \kappa_{10} = \kappa_{13} = 1,\\ &\kappa_3 = \frac{\epsilon_c\lambda_m^* S_c^*}{\eta_c E_c^*},\quad \kappa_4 = \frac{\tau_c R_c^*}{r_c I_c^*},\quad \kappa_7 = \frac{\lambda_m^* S_m^*}{\eta_m E_m^*},\quad \kappa_8 = \frac{\tau_m R_m^*}{r_m I_m^*},\\ &\kappa_{11} = \frac{\lambda_l^* S_l^*}{\eta_l E_l^*},\quad \kappa_{12} = \frac{\tau_l R_l^*}{r_l I_l^*}. \qquad (17)\end{aligned}$$

Substituting Equation 17 into Equation 16 and simplifying, we have

$$\begin{aligned}\frac{d\mathscr{L}}{dt} &= -k_1 S_c\left(1-\frac{1}{b}\right)^2 - \mu_h S_m\left(1-\frac{1}{g}\right)^2 \\ &+ \epsilon_c\lambda_m^* S_c^*\left(3+a-e-\frac{d}{e}-\frac{ab}{d}-\frac{1}{b}\right) \\ &+ \lambda_m^* S_m^*\left(3+a-m-\frac{h}{m}-\frac{ag}{h}-\frac{1}{g}\right) \\ &+ \lambda_l^* S_l^*\left(3+p-x-\frac{u}{x}-\frac{pq}{u}-\frac{1}{q}\right) \\ &+ \phi_c I_c^*\left(1+e-z-\frac{e}{z}\right)+\phi_m I_m^*\left(1+m-z-\frac{m}{z}\right) \\ &+ \phi_l I_l^*\left(1+x-z-\frac{x}{z}\right) \\ &+ \beta_c S_c^*\left(b+\frac{1}{g}-\frac{b}{g}-1\right) \\ &+ \tau_c R_c^*\left(e+\frac{1}{b}-\frac{f}{b}-\frac{e}{f}\right)+\tau_m R_m^*\left(m+\frac{1}{g}-\frac{n}{g}-\frac{m}{n}\right) \\ &+ \tau_l R_l^*\left(x+\frac{1}{q}-\frac{y}{q}-\frac{x}{y}\right).\end{aligned}$$

Consider $v(x) = 1 - x + \ln(x) \leq 0$ for any $x > 0$ with equality holding if $x = 1$. For $1 - x \leq -\ln(x)$, we realize that

$$\begin{aligned}3 &+ a - e - \frac{d}{e} - \frac{ab}{d} - \frac{1}{b} \\ &= (1-e)+\left(1-\frac{d}{e}\right)+\left(1-\frac{ab}{d}\right)+\left(1-\frac{1}{b}\right)-(1-a) \\ &\leq -\ln(e)-\ln\left(\frac{d}{e}\right)-\ln\left(\frac{ab}{d}\right)-\ln\left(\frac{1}{b}\right)+\ln(a) \\ &= \ln\left(\frac{1}{e}\cdot\frac{e}{d}\cdot\frac{d}{ab}\cdot b\cdot a\right)=0,\end{aligned}$$

$$\begin{aligned}1 &+ e - z - \frac{e}{z} \\ &= (1-z)+\left(1-\frac{e}{z}\right)-(1-e) \\ &\leq -\ln(z)-\ln\left(\frac{e}{z}\right)+\ln(e)=\ln\left(\frac{1}{z}\cdot\frac{z}{e}\cdot e\right)=0,\end{aligned}$$

$$\begin{aligned}b &+ \frac{1}{g} - \frac{b}{g} - 1 \\ &= \left(1-\frac{b}{g}\right)-\left(1-\frac{1}{g}\right)-(1-b) \\ &\leq -\ln\left(\frac{b}{g}\right)+\ln\left(\frac{1}{g}\right)+\ln(b)=\ln\left(\frac{g}{b}\cdot\frac{1}{g}\cdot b\right)=0,\end{aligned}$$

and

$$\begin{aligned}e &+ \frac{1}{b} - \frac{f}{b} - \frac{e}{f} \\ &= \left(1-\frac{f}{b}\right)+\left(1-\frac{e}{f}\right)-\left(1-\frac{1}{b}\right)-(1-e) \\ &\leq -\ln\left(\frac{f}{b}\right)-\ln\left(\frac{e}{f}\right)+\ln\left(\frac{1}{b}\right)+\ln(e) \\ &= \ln\left(\frac{b}{f}\cdot\frac{f}{e}\cdot\frac{1}{b}\cdot e\right)=0.\end{aligned}$$

Following the same procedure, we see that

$$\begin{aligned}\left(3+a-m-\frac{h}{m}-\frac{ag}{h}-\frac{1}{g}\right) &\leq 0, \quad \left(3+p-x-\frac{u}{x}-\frac{pq}{u}-\frac{1}{q}\right) \\ &\leq 0, \left(1+m-z-\frac{m}{z}\right)\leq 0, \\ \left(1+x-z-\frac{x}{z}\right) &\leq 0, \quad \left(m+\frac{1}{g}-\frac{n}{g}-\frac{m}{n}\right)\leq 0, \\ &\text{and} \quad \left(x+\frac{1}{q}-\frac{y}{q}-\frac{x}{y}\right)\leq 0.\end{aligned}$$

Hence,

$$\frac{d\mathscr{L}}{dt} \leq 0,$$

with equality holding if and only if $a = b = d = e = f = g = h = m = n = p = q = u = x = y = z = 1$, which corresponds precisely to the set $\Omega = \Omega^*$. It follows that the endemic equilibrium E^* constitutes the maximal invariant subset of Ω.

Invoking LaSalle's invariance principle [24], we deduce that, as $t \to \infty$, every solution of Equation 6 converges to the endemic equilibrium E^* whenever $\mathcal{R}_0 > 1$. Consequently, within the invariant region Ω, the equilibrium point $E^*$is globally asymptotically stable. □

3 Stochastic model

Biological processes are inherently variable, and this variability becomes especially important in the study of infectious diseases, where random fluctuations can shift the course of transmission. Deterministic models describe the average progression of infection but cannot capture the discrete and unpredictable movements of individuals between epidemiological states. In contrast, stochastic models incorporate demographic randomness by treating the number of individuals in each compartment as integer-valued quantities that evolve through probabilistic events over continuous time [25, 26].

A key implication of demographic randomness is that the final infectious individual in a population may clear the infection before generating any secondary cases. Consequently, extinction of giardiasis can occur purely due to chance, even when the deterministic model predicts persistence. Deterministic trajectories may also allow infection levels below a single individual, which is biologically unrealistic; stochastic formulations avoid this by enforcing transitions only between whole-number states [27, 28].

Random fluctuations can be particularly pronounced for giardiasis due to the multiple transmission routes involving immunocompetent humans, immunocompromised humans, lambs, and cysts contaminating the environment. These interactions create opportunities for the pathogen to fade out or re-establish, depending on the timing and sequence of events. Because stochastic models allow estimation of extinction probabilities and the distribution of extinction times [25, 26], they provide an essential complement to the deterministic analysis of Section 2.

For these reasons, we formulate a continuous-time Markov chain (CTMC) model that preserves the compartmental structure

and assumptions of the deterministic system but treats all transitions as random events occurring at specified rates. This allows for a more realistic exploration of giardiasis dynamics in finite populations.

3.1 Giardiasis CTMC stochastic model formulation

The stochastic version of the model extends the deterministic Equation 6 by treating all state variables as integer-valued processes that evolve randomly over time [25, 29]. To formulate the continuous-time Markov chain (CTMC), we define the state vector

$$X(t) = \big(S_c(t), E_c(t), I_c(t), R_c(t), S_m(t), E_m(t), I_m(t), R_m(t),\ S_l(t), E_l(t), I_l(t), R_l(t), G_p(t)\big),$$

for $t \geq 0$ and where S_c, E_c, I_c, R_c corresponds to immunocompetent humans, S_m, E_m, I_m, R_m to immunocompromised humans, S_l, E_l, I_l, R_l to lambs, and G_p to environmental Giardia cysts. Each component is assumed to take values in the finite set

$$\{0, 1, 2, \ldots, \mathcal{N}\},$$

with $\mathcal{N} \in \mathbb{Z}_+$ representing a sufficiently large upper bound on the population size.

The CTMC is assumed to be time-homogeneous, meaning transition rates depend only on the current state and not on time explicitly [29]. Each transition in the CTMC corresponds to a biologically meaningful event such as infection, progression, recovery, loss of immunity, natural death, disease-induced death, shedding of cysts, or environmental clearance. Every event changes one or more entries of $X(t)$ by ± 1, while all other components remain fixed. The rate at which a given event occurs is derived directly from the deterministic formulation. For example, susceptible immunocompetent humans acquire infection at a rate $\lambda_c S_c$, where

$$\lambda_m = \theta_c I_c + \theta_m I_m + \theta_l I_l + \theta_p G_p, \qquad \lambda_c = \epsilon_c \lambda_m, \qquad \lambda_l = \kappa_l I_l + \kappa_p G_p,$$

as given earlier in Equations 3–5. Exposed lambs progress to the infectious class at rate $\eta_l E_l$, and cysts are removed from the environment at rate $\mu_p G_p$. A complete list of transitions and their associated rates is provided in Table 2.

For a fixed time t, the random state $X(t)$ takes values in the finite state space

$$\mathcal{S} = \{0, 1, \ldots, \mathcal{N}\}^{13},$$

and its probability mass function is defined by

$$P_\phi(t) = \Pr\{X(t) = \phi\},$$

for any admissible state

$$\phi = (s_c, e_c, i_c, r_c,\ s_m, e_m, i_m, r_m,\ s_l, e_l, i_l, r_l,\ g_p) \in \mathcal{S}.$$

We assume that the process is time-homogeneous and satisfies the Markov property:

$$\Pr\{X(t + \Delta t) \mid X(0), X(\Delta t), \ldots, X(t)\} = \Pr\{X(t + \Delta t) \mid X(t)\},$$

for all $t \geq 0$ and any $\Delta t > 0$. Consequently, the waiting time between successive events is exponentially distributed, and in a sufficiently small interval $[t, t + \Delta t)]$ we may assume that at most one transition occurs.

Let ν_k denote the jump vector corresponding to a specific admissible event, and let $a_k(x)$ denote its transition rate when the system is in state x. The infinitesimal transition probabilities are then

$$\begin{aligned} P_{x+\nu_k, x}(\Delta t) &= a_k(x)\,\Delta t + o(\Delta t), \\ P_{x,x}(\Delta t) &= 1 - \xi(x)\Delta t + o(\Delta t), \end{aligned} \tag{18}$$

where

$$\xi(x) = \sum_k a_k(x)$$

is the total rate at which any event can occur from state x. All other transitions occur with probability $o(\Delta t)$.

Using the rates in Table 2, the total rate $\xi(x)$ can be written explicitly as

$$\begin{aligned} \xi(x) \quad &= \sigma_c \Lambda_h + (1 - \sigma_c)\Lambda_h + \Lambda_l + \lambda_c s_c + \lambda_m s_m \\ &\quad + \lambda_l s_l + \beta_c s_c + \tau_c r_c + \tau_m r_m + \tau_l r_l \\ &\quad + \eta_c e_c + \eta_m e_m + \eta_l e_l + r_c i_c + r_m i_m + r_l i_l \\ &\quad + (\mu_h + d_c) i_c + (\mu_h + d_m) i_m + (\mu_l + d_l) i_l \\ &\quad + \mu_h(s_c + e_c + r_c) + \mu_h(s_m + e_m + r_m) \\ &\quad + \mu_l(s_l + e_l + r_l) + \phi_c i_c + \phi_m i_m + \phi_l i_l + \mu_p g_p. \end{aligned} \tag{19}$$

Let $P_x(t) = \Pr\{X(t) = x\}$. Using the Markov property and the infinitesimal transition relations (Equation 18), we obtain

$$P_x(t + \Delta t) = \sum_{k:\, x - \nu_k \in \mathcal{S}} P_{x, x-\nu_k}(\Delta t)\, P_{x-\nu_k}(t) + P_{x,x}(\Delta t)\, P_x(t),$$

and by letting $\Delta t \to 0$ we arrive at the forward Kolmogorov (master) equation:

$$\frac{dP_x(t)}{dt} = \sum_{k:\, x - \nu_k \in \mathcal{S}} a_k(x - \nu_k)\, P_{x-\nu_k}(t) - \xi(x)\, P_x(t), \tag{20}$$

for all $x \in \mathcal{S}$, with $\xi(x)$ given in Equation 19. Biologically, Equation 20 expresses that the probability of occupying a given state increases due to transitions into the state and decreases due to transitions out of the state. The disease-free state $0 = (0, \ldots, 0)$ is an absorbing state of the CTMC; once entered, the process remains there indefinitely and giardiasis has gone extinct.

The CTMC framework retains the biological structure of the deterministic model while incorporating demographic variability. It permits computation of extinction probabilities, outbreak likelihood, and the distribution of extinction times, and forms the basis for the branching process approximation developed in the next section.

TABLE 2 State transitions and corresponding occurrence rates for the giardiasis CTMC stochastic model.

Event	State transition	Rate
Recruitment of S_c	$(S_c,\ldots,G_p)\to(S_c+1,\ldots,G_p)$	$\sigma_c\Lambda_h$
Recruitment of S_m	$(S_c,\ldots,S_m,\ldots,G_p)\to(S_c,\ldots,S_m+1,\ldots,G_p)$	$(1-\sigma_c)\Lambda_h$
Recruitment of S_l	$(\ldots,S_l,\ldots,G_p)\to(\ldots,S_l+1,\ldots,G_p)$	Λ_l
Loss of immunity in R_c	$(S_c,\ldots,R_c,\ldots,G_p)\to(S_c+1,\ldots,R_c-1,\ldots,G_p)$	$\tau_c R_c$
Loss of immunity in R_m	$(\ldots,S_m,\ldots,R_m,\ldots)\to(\ldots,S_m+1,\ldots,R_m-1,\ldots)$	$\tau_m R_m$
Loss of immunity in R_l	$(\ldots,S_l,\ldots,R_l,G_p)\to(\ldots,S_l+1,\ldots,R_l-1,G_p)$	$\tau_l R_l$
Infection of S_c	$(S_c,E_c,\ldots)\to(S_c-1,E_c+1,\ldots)$	$\lambda_c S_c$
Infection of S_m	$(\ldots,S_m,E_m,\ldots)\to(\ldots,S_m-1,E_m+1,\ldots)$	$\lambda_m S_m$
Infection of S_l	$(\ldots,S_l,E_l,\ldots)\to(\ldots,S_l-1,E_l+1,\ldots)$	$\lambda_l S_l$
Progression $E_c\to I_c$	$(\ldots,E_c,I_c,\ldots)\to(\ldots,E_c-1,I_c+1,\ldots)$	$\eta_c E_c$
Progression $E_m\to I_m$	$(\ldots,E_m,I_m,\ldots)\to(\ldots,E_m-1,I_m+1,\ldots)$	$\eta_m E_m$
Progression $E_l\to I_l$	$(\ldots,E_l,I_l,\ldots)\to(\ldots,E_l-1,I_l+1,\ldots)$	$\eta_l E_l$
Recovery of I_c	$(\ldots,I_c,R_c,\ldots)\to(\ldots,I_c-1,R_c+1,\ldots)$	$r_c I_c$
Recovery of I_m	$(\ldots,I_m,R_m,\ldots)\to(\ldots,I_m-1,R_m+1,\ldots)$	$r_m I_m$
Recovery of I_l	$(\ldots,I_l,R_l,G_p)\to(\ldots,I_l-1,R_l+1,G_p)$	$r_l I_l$
Natural death of S_c	$(S_c,\ldots)\to(S_c-1,\ldots)$	$\mu_h S_c$
Natural death of E_c	$(\ldots,E_c,\ldots)\to(\ldots,E_c-1,\ldots)$	$\mu_h E_c$
Natural death of I_c	$(\ldots,I_c,\ldots)\to(\ldots,I_c-1,\ldots)$	$\mu_h I_c$
Natural death of R_c	$(\ldots,R_c,\ldots)\to(\ldots,R_c-1,\ldots)$	$\mu_h R_c$
Natural death of S_m	$(\ldots,S_m,\ldots)\to(\ldots,S_m-1,\ldots)$	$\mu_h S_m$
Natural death of E_m	$(\ldots,E_m,\ldots)\to(\ldots,E_m-1,\ldots)$	$\mu_h E_m$
Natural death of I_m	$(\ldots,I_m,\ldots)\to(\ldots,I_m-1,\ldots)$	$\mu_h I_m$
Natural death of R_m	$(\ldots,R_m,\ldots)\to(\ldots,R_m-1,\ldots)$	$\mu_h R_m$
Natural death of S_l	$(\ldots,S_l,\ldots)\to(\ldots,S_l-1,\ldots)$	$\mu_l S_l$
Natural death of E_l	$(\ldots,E_l,\ldots)\to(\ldots,E_l-1,\ldots)$	$\mu_l E_l$
Natural death of I_l	$(\ldots,I_l,\ldots)\to(\ldots,I_l-1,\ldots)$	$\mu_l I_l$
Natural death of R_l	$(\ldots,R_l,G_p)\to(\ldots,R_l-1,G_p)$	$\mu_l R_l$
Disease–induced death of I_c	$(\ldots,I_c,\ldots)\to(\ldots,I_c-1,\ldots)$	$d_c I_c$
Disease–induced death of I_m	$(\ldots,I_m,\ldots)\to(\ldots,I_m-1,\ldots)$	$d_m I_m$
Disease–induced death of I_l	$(\ldots,I_l,\ldots)\to(\ldots,I_l-1,\ldots)$	$d_l I_l$
Shedding of cysts by I_c	$(\ldots,I_c,\ldots,G_p)\to(\ldots,I_c,\ldots,G_p+1)$	$\phi_c I_c$
Shedding of cysts by I_m	$(\ldots,I_m,\ldots,G_p)\to(\ldots,I_m,\ldots,G_p+1)$	$\phi_m I_m$
Shedding of cysts by I_l	$(\ldots,I_l,\ldots,G_p)\to(\ldots,I_l,\ldots,G_p+1)$	$\phi_l I_l$
Environmental clearance of cysts	$(\ldots,G_p)\to(\ldots,G_p-1)$	$\mu_p G_p$

The state vector is $X=(S_c,E_c,I_c,R_c,S_m,E_m,I_m,R_m,S_l,E_l,I_l,R_l,G_p)$.

3.2 Multiple branching process

The early stages of giardiasis transmission are driven by chance events because the number of newly infected individuals is initially small, and each infectious individual may or may not generate additional cases before recovering or dying. To capture this randomness and to approximate the behavior of the CTMC model near the disease-free state, we formulate a multitype branching process. This approach has been widely applied in stochastic epidemic modeling for protozoan infections and zoonoses [16, 22], and provides a tractable way to study the probability of outbreak establishment and the distribution of early transmission chains.

The deterministic Equation 6 describes three epidemiologically distinct host classes (immunocompetent humans, immunocompromised humans, and lambs), together with an environmental reservoir of cysts. Each of these components contributes to onward transmission, either through direct host-to-host contact or through the shedding and acquisition of Giardia cysts. The CTMC model of Section 3.1 represents these interactions through random event rates. When infection is rare, however,

the susceptibles remain approximately constant, and transitions among the infected compartments are driven solely by the random behavior of a small number of infectious individuals. Under these circumstances, the CTMC dynamics can be approximated by a multitype branching process, where each infectious individual (or cyst) produces "offspring" of various types according to probability laws determined by the transition rates.

We classify infectious entities into four types corresponding to the transmission-generating components of types 1–4, where Type 1 is infectious immunocompetent humans (I_c), Type 2 is infectious immunocompromised humans (I_m), Type 3 is infectious lambs (I_l), and Type 4 is viable Giardia cysts in the environment (G_p). During its infectious period, a Type 1 individual may generate new exposed humans (E_c or E_m), infect lambs through environmental contamination, or contribute to cyst production. Analogous statements hold for Types 2 and 3. Type 4 (cysts) generates new infections in all host classes at rates proportional to θ_p and κ_p as defined in Equations 3–5. Because susceptibles remain effectively constant during the threshold phase, the resulting infection events correspond to "offspring" of new types, where each primary infectious individual initiates an independent transmission chain [26, 30].

Let $Z_n = (Z_n^{(1)}, Z_n^{(2)}, Z_n^{(3)}, Z_n^{(4)})$ denote the number of individuals of each type in generation n. The process $\{Z_n\}_{n\geq 0}$ forms a four-type Galton-Watson branching process with mean offspring matrix $M = (m_{ij})$, where m_{ij} is the expected number of type-j offspring produced by a single type-i individual.

For $i = 1$ (immunocompetent humans), an infectious period lasting on average $1/(r_c+\mu_h+d_c)$ produces new immunocompetent infections at rate $\epsilon_c\theta_c$, infections in immunocompromised humans at rate $\epsilon_c\theta_m$, lamb infections through the environment via progression to cysts at rate φ_c followed by environmental acquisition κ_p, and new cysts directly at rate φ_c.

Thus,

$$m_{1j} = \int_0^\infty \text{rate}_{1\to j}(t)\, S_{\text{surv}}^{(1)}(t)\, dt,$$

where $S_{\text{surv}}^{(1)}(t)$ is the probability the infectious period of a type 1 individual exceeds time t.

Similar reasoning yields expressions for m_{2j} and m_{3j}, replacing the appropriate parametric rates $\{\theta_m, \eta_m, r_m, \varphi_m\}$ and $\{\kappa_l, \eta_l, r_l, \varphi_l\}$, respectively. Type 4 cysts have an exponential lifetime with rate μ_p, during which they may generate human or lamb exposures at rates $\{\theta_p, \kappa_p\}$, giving

$$m_{4j} = \frac{\text{rate}_{4\to j}}{\mu_p}.$$

The full matrix M therefore takes the form

$$M = \begin{pmatrix} m_{11} & m_{12} & m_{13} & m_{14} \\ m_{21} & m_{22} & m_{23} & m_{24} \\ m_{31} & m_{32} & m_{33} & m_{34} \\ m_{41} & m_{42} & m_{43} & m_{44} \end{pmatrix},$$

where all entries are non-negative and depend solely on the infection and progression rates of Equation 6. Closed-form expressions can be derived in terms of the model parameters, analogous to the construction of next-generation matrices in deterministic models [19, 20].

The dominant eigenvalue $\rho(M)$ of the mean offspring matrix determines the behavior of the branching process, such that $\rho(M) < 1$ implies that extinction occurs with probability 1, and $\rho(M) > 1$ implies positive probability of outbreak establishment [28, 30].

The extremely low extinction probability associated with introductions through the environmental cyst class G_p reflects the role of sustained environmental loading rather than a single fixed numerical concentration threshold. In the stochastic framework, the transition from fade-out to a sustained outbreak occurs when cyst-driven transmission increases the dominant eigenvalue of the mean offspring matrix beyond unity, which corresponds to the deterministic threshold $\mathcal{R}_0 > 1$. Biologically, this implies that persistence depends on the balance between cyst shedding (ϕ_c, ϕ_m, ϕ_l), environmental acquisition (θ_p, κ_p), and cyst decay (μ_p). When shedding and acquisition rates collectively outweigh environmental clearance, cyst concentrations remain sufficiently high over time to generate secondary infections faster than stochastic extinction removes them. Thus, even moderate initial cyst levels may trigger a sustained outbreak if environmental persistence is strong, whereas rapid decay or reduced shedding can keep the system below the effective persistence threshold. This interpretation explains why introductions via G_p produce markedly lower extinction probabilities and highlights the importance of interventions that reduce environmental contamination to prevent the system from crossing the outbreak boundary.

This threshold agrees with the basic reproduction number of the deterministic model, a relationship established in similar CTMC formulations for zoonotic and environmental pathogens [16, 22]. When infection is rare, the susceptible populations remain close to their disease-free equilibrium values, so the branching process provides an accurate approximation to the CTMC until the number of infectious individuals becomes large.

Furthermore, Giardia cysts contribute significantly to the amplification of infection chains, and their inclusion as a distinct type is essential. A single infectious host may shed many cysts, each capable of causing new infections before clearance. Such "burst" behavior is well captured by branching processes and is consistent with observations reported for other environmentally mediated protozoan diseases [22]. This enhances the offspring variance and increases the possibility that a small number of initial cases may trigger a sustained outbreak even when $\rho(M)$ is close to 1.

The multitype branching process serves two key roles in later analysis: (i) it provides explicit formulas for extinction probabilities of giardiasis when infection is introduced by a small number of hosts or cysts; and (ii) it forms the basis for deriving the stochastic threshold discussed in Section 3.1. The branching framework also facilitates sensitivity analyses, particularly with respect to shedding rates and environmental transmission parameters, which are addressed in Section 4.

3.2.1 Stochastic threshold for the CTMC stochastic model

In the earliest phase of giardiasis invasion, only a very small number of infectious individuals or cysts are present. The

susceptible populations thus remain effectively constant at their disease-free equilibrium levels, and the nonlinear feedbacks in the CTMC can be neglected. Under this approximation, the dynamics of new infections are well described by a multitype branching process, as introduced in Section 3.2. The branching representation enables explicit calculation of extinction probabilities and provides a rigorous definition of the *stochastic threshold*, which determines whether giardiasis is likely to fade out or establish a major outbreak.

Let the four types of infectious entities be indexed as follows:

$$1 = I_c, \qquad 2 = I_m, \qquad 3 = I_l, \qquad 4 = G_p.$$

For each type $i \in \{1, 2, 3, 4\}$, let X_{ij} denote the number of type-j "offspring" generated by a single type-i entity during its infectious or viable period. The offspring probability generating function (pgf) for type i is then defined as

$$G_i(s_1, s_2, s_3, s_4) = \mathbb{E}\left[s_1^{X_{i1}} s_2^{X_{i2}} s_3^{X_{i3}} s_4^{X_{i4}}\right].$$

These pgfs encode all of the probabilistic structure of the branching process. Because infection, progression, recovery, and shedding events occur at fixed exponential rates (Section 3.1), the underlying waiting times are memoryless, and the counts of offspring of each type are Poisson-distributed. Thus, each G_i has the exponential-Poisson form

$$G_i(\mathbf{s}) = \exp\left(\sum_{j=1}^{4} m_{ij}(s_j - 1)\right),$$

where m_{ij} is the mean number of type-j offspring produced by one type-i individual. These mean values are determined directly from the transition rates in Equation 6: infection rates $\lambda_c, \lambda_m, \lambda_l$, cyst shedding rates $\varphi_c, \varphi_m, \varphi_l$, and environmental acquisition rates θ_p, κ_p yield the expected offspring contributed by each pathway.

Collecting the coefficients m_{ij} produces the 4×4 mean matrix

$$M = \begin{pmatrix} m_{11} & m_{12} & m_{13} & m_{14} \\ m_{21} & m_{22} & m_{23} & m_{24} \\ m_{31} & m_{32} & m_{33} & m_{34} \\ m_{41} & m_{42} & m_{43} & m_{44} \end{pmatrix},$$

where, for example,

$$m_{14} = \frac{\varphi_c}{r_c + \mu_h + d_c}, \qquad m_{41} = \frac{\theta_p S_c^0}{\mu_p},$$

with S_c^0 denoting the susceptible immunocompetent population at the disease-free equilibrium. Similar expressions hold for the other entries, using the appropriate parameter combinations for immunocompromised humans and lambs. This structure is analogous to next-generation matrices used in deterministic models [19, 20], but here it captures the reproduction of *infectious individuals* rather than infected *flows*.

To capture the extinction probabilities of giardiasia, we let q_i be the probability that giardiasis eventually goes extinct when the process starts with a single type-i individual. Standard results for multitype branching processes imply that the extinction probability vector

$$q = (q_1, q_2, q_3, q_4)$$

is the minimal nonnegative solution of the system

$$q_i = G_i(q_1, q_2, q_3, q_4), \qquad i = 1, \ldots, 4.$$

In vector notation,

$$q = G(q),$$

where $G = (G_1, \ldots, G_4)$ is the pgf vector. The system always has the trivial solution $q = (1, 1, 1, 1)$, representing almost-sure extinction. A second, nontrivial solution exists with at least one $q_i < 1$ exactly when the branching process is supercritical.

The branching process is classified by the spectral radius $\rho(M)$ of the offspring mean matrix: $\rho(M) < 1$ which implies subcritical process, extinction with probability 1, $\rho(M) = 1$ which implies critical process, extinction with probability 1 but slow, and $\rho(M) > 1$ which implies supercritical process, positive probability of outbreak.

This threshold criterion is consistent with the Perron–Frobenius theorem and has been applied in similar stochastic models of protozoan and zoonotic diseases [22, 31, 32]. When $\rho(M) > 1$, the pgf system admits a nontrivial extinction probability vector q satisfying $q_i < 1$ for at least one type i, indicating a genuine chance of giardiasis invasion.

The deterministic threshold R_0 of Equation 6 and the stochastic threshold $\rho(M)$ coincide in the sense that

$$R_0 > 1 \iff \rho(M) > 1.$$

However, the interpretations differ: $R_0 > 1$ guarantees *deterministic* invasion, whereas $\rho(M) > 1$ implies only that a major outbreak is *possible*, not certain. Random fade-out can still occur. This distinction is particularly important for giardiasis, where environmental amplification and heterogeneous host responses produce substantial variation in early transmission chains, as observed in comparable systems [31].

The stochastic threshold $\rho(M) = 1$ therefore provides the appropriate criterion for giardiasis invasion in finite populations. It forms the basis for the extinction probability analysis of Section 4 and for assessing how shedding rates, environmental contamination, and host susceptibility influence the likelihood of eliminating or establishing the disease.

4 Numerical simulation

This section investigates the numerical behavior of the deterministic giardiasis model formulated in Section 2 and its corresponding CTMC stochastic analog developed in Section 3. Numerical simulation serves two main purposes. First, it validates the internal consistency of the stochastic formulation by comparing its expected trajectories with the deterministic system. Second, it provides insight into the variability of stochastic sample paths, extinction tendencies, and the influence of heterogeneity in shedding and environmental contamination.

Following the approach in Mgandu et al. [22] and Charles et al. [16], we simulate both models under identical biological parameters and initial conditions. The deterministic system is solved using

a stiff ODE solver, while the stochastic system is approximated using Gillespie's direct algorithm. The comparison of these outputs provides an empirical foundation for Sections 4.2–4.4, where extinction probabilities, shedding sensitivity, and stochastic threshold behavior are analyzed in detail.

Parameter values are chosen from published epidemiological literature, giardiasis field studies, and related protozoan transmission models. When empirical estimates are not available, reasonable values are adopted following methods in Mgandu et al. [22] and Luhanda et al. [31] and sensitivity-tested in later subsections. The complete list of parameter values used in all numerical experiments is presented in Table 3.

TABLE 3 Model parameter values.

Parameter	Value	Source
σ_c	0.96933871	[35]
τ_m	0.07573930	[36]
Λ_h	10,000/24,090	[37]
d_m	0.00001199	[35]
τ_c	0.05388403	[36]
r_m	1/18.5	[35]
ϵ_c	1/3	[38]
Λ_l	400/365	[37]
θ_c	0.00001166	[35]
r_l	0.05579842	[35]
θ_m	0.00002135	[35]
κ_l	0.00003018	[38]
θ_l	0.00003153	[35]
κ_p	0.00003478	[38]
θ_p	0.00003301	[35]
μ_l	1/2,190	[37]
β_c	0.00000137	[35, 36]
η_l	1/6	[36]
μ_h	1/24,090	[37]
r_c	1/14	[35]
η_c	1/13	[36]
d_l	0.00017815	[35]
η_m	1/7	[36]
ϕ_c	0.02257157	[35, 38]
d_c	0.00000145	[35]
ϕ_m	0.030072500	[35, 38]
r_c	1/14	[35]
ϕ_l	0.45572367	[35, 38]
μ_p	0.04139149	[37]

4.1 Deterministic and CTMC stochastic model simulations

We begin by numerically solving the deterministic Equation 6 introduced in Section 2 and analyzed in Section 3 and comparing its behavior with multiple stochastic realizations of the CTMC model. The purpose is to verify that the CTMC sample mean approximates the deterministic trajectory, while individual stochastic paths reveal fluctuations and potential fade-out not captured by the ODE model. Such comparisons are standard in stochastic epidemic analysis [16, 25, 33].

Table 3 lists the biological and epidemiological parameters used in the numerical experiments. These include human recruitment, lamb recruitment, natural mortality, progression rates, shedding intensities, environmental decay, and infection rates described in Section 2. The parameter set is fixed throughout Sections 4.1–4.4 unless otherwise stated.

Numerical results are independent of specific magnitudes, as subsequent subsections will incorporate sensitivity testing analogous to the procedures used in Mgandu et al. [22].

The simulations use the following initial conditions at time $t = 0$:

$$S_c(0) = S_c^0,\ E_c(0) = 0,\ I_c(0) = 1,\ R_c(0) = 0,$$

$$S_m(0) = S_m^0,\ E_m(0) = 0,\ I_m(0) = 0,\ R_m(0) = 0,$$

$$S_l(0) = S_l^0,\ E_l(0) = 0,\ I_l(0) = 0,\ R_l(0) = 0,\ G_p(0) = 0.$$

These reflect the introduction of a single human infection into an otherwise disease-free population, consistent with Section 3.2.1 and the outbreak-initiation scenarios used in Mgandu et al. [22]. The total susceptible populations S_c^0, S_m^0, and S_l^0 correspond to the disease-free equilibrium values.

Following the numerical approach in Luhanda et al. [31] and Mgandu et al. [22], the deterministic system is solved over the interval $[0, 500]$ days using MATLAB's stiff solver `ode15s` with relative and absolute tolerances set to 10^{-8}, following recommended practice for stiff environmental pathogen systems [34]. For the CTMC model, Gillespie's direct algorithm is implemented with an event-driven time increment determined by the total reaction propensity. Although $N = 500$ stochastic realizations are generated for statistical analysis, only three representative sample paths are displayed in Figures 2–8 to facilitate comparison with the deterministic trajectories. The CTMC trajectories and deterministic solution are interpolated onto a uniform time grid of $\Delta t = 0.01$ days for plotting, ensuring consistent visual comparison across all state variables.

Across all epidemiological classes, the deterministic solution lies close to the mean of the stochastic paths, while the individual CTMC trajectories reveal variability arising from early outbreak fade-out, demographic randomness, and fluctuations in cyst accumulation. In particular, several sample paths show minimal deviation from their initial susceptible values due to stochastic extinction occurring before sustained transmission is established. This behavior mirrors observations made for cryptosporidiosis in Luhanda et al. [31] and rabies transmission in Charles et al. [16]. The combined results, shown in Figures 2–8, confirm strong agreement between deterministic and stochastic dynamics in high-prevalence regimes and highlight the importance of stochastic fade-out in low-infection scenarios.

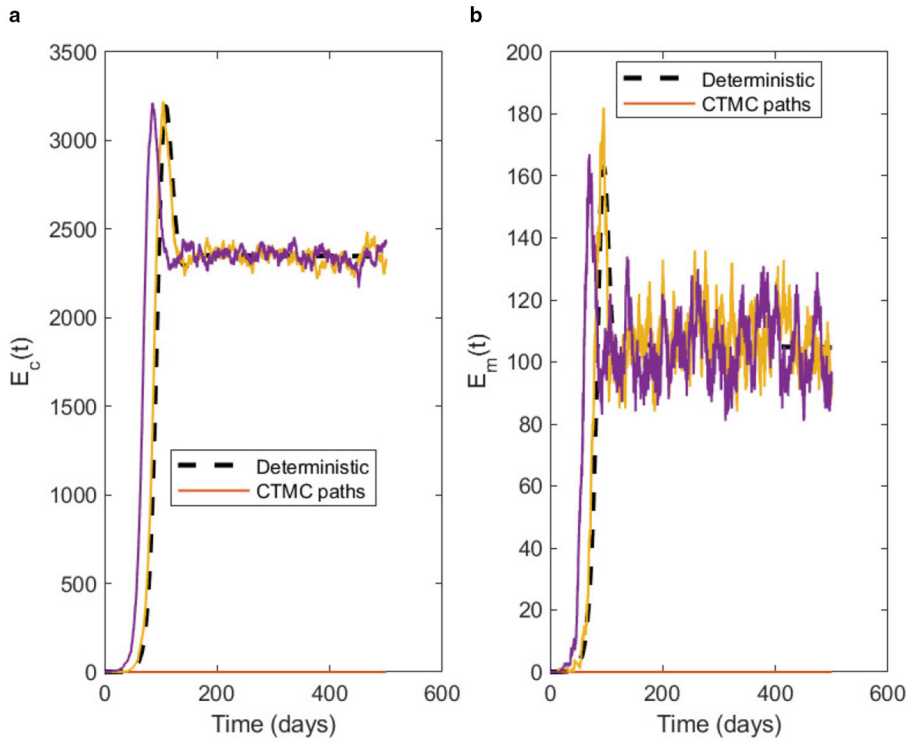

FIGURE 3
Sample realizations of the CTMC stochastic process (solid lines) alongside the corresponding deterministic trajectories (dashed lines) for **(a)** exposed immunocompetent humans E_c and **(b)** exposed immunocompromised humans E_m. Solid curves represent multiple stochastic realizations of the CTMC model, included to illustrate demographic randomness and variability in outbreak trajectories, while dashed curves denote the corresponding deterministic solution.

4.2 Probability of giardiasis extinction and comparison of deterministic and stochastic dynamics

In this subsection, we investigate the extinction behavior of giardiasis in the continuous-time Markov chain (CTMC) formulation of the model, following the multitype branching process framework described in Luhanda et al. [31]. The infectious classes (I_c, I_m, I_ℓ, G_p) constitute the "types" of the branching process, and the associated mean offspring matrix M is constructed using the linearised CTMC transition structure at the giardiasis disease-free equilibrium (GDFE) E^0 given in Equation 13.

Let $\mathbf{q} = (q_1, q_2, q_3, q_4)$ denote the minimal non-negative fixed point of the probability-generating function associated with the branching process. The quantity

$$P_0 = q_i$$

represents the probability of disease extinction when the outbreak is initiated in the infectious class i, with one individual introduced into that class and all other infectious classes starting at zero.

Using the parameter set in Table 1 and the fixed-point equation

$$\mathbf{q} = f(\mathbf{q}),$$

The extinction probabilities P_0 for each of the four infectious classes were computed. Table 4 summarizes the exact extinction probabilities P_0 and the approximate values P_a obtained using the CTMC numerical simulation procedure.

The results indicate a strong dependence of extinction probability on the entry compartment. When the infection emerges from an immunocompetent human (I_c), the extinction probability is relatively high ($P_0 \approx 0.542$). A smaller extinction probability is observed for outbreaks initiated in immunocompromised humans (I_m). However, the extinction probability becomes extremely small when giardiasis is introduced through the lamb infectious class (I_ℓ) or from the environmental cyst class (G_p), suggesting that environmental and livestock reservoirs play a dominant role in sustaining transmission. A simultaneous introduction of infection in all four infectious classes yields an extinction probability close to zero, implying a near-certain major outbreak.

To further illustrate the stochastic behavior of the system, we simulated multiple CTMC sample paths together with the deterministic solution of Equation 6. Figure 9 displays five CTMC sample paths for the infectious classes (I_c, I_m, I_ℓ) and the environmental cysts G_p, superimposed with the deterministic trajectory. As in Luhanda et al. [31], the stochastic paths exhibit noticeable fluctuations during the early phase of infection, after which they stabilize around the deterministic solution. This behavior reflects the fact that demographic noise is most significant when the number of infectious individuals is small, but its relative impact diminishes as the epidemic grows.

Importantly, none of the stochastic paths in the simulations fell to zero within the observation window, consistent with

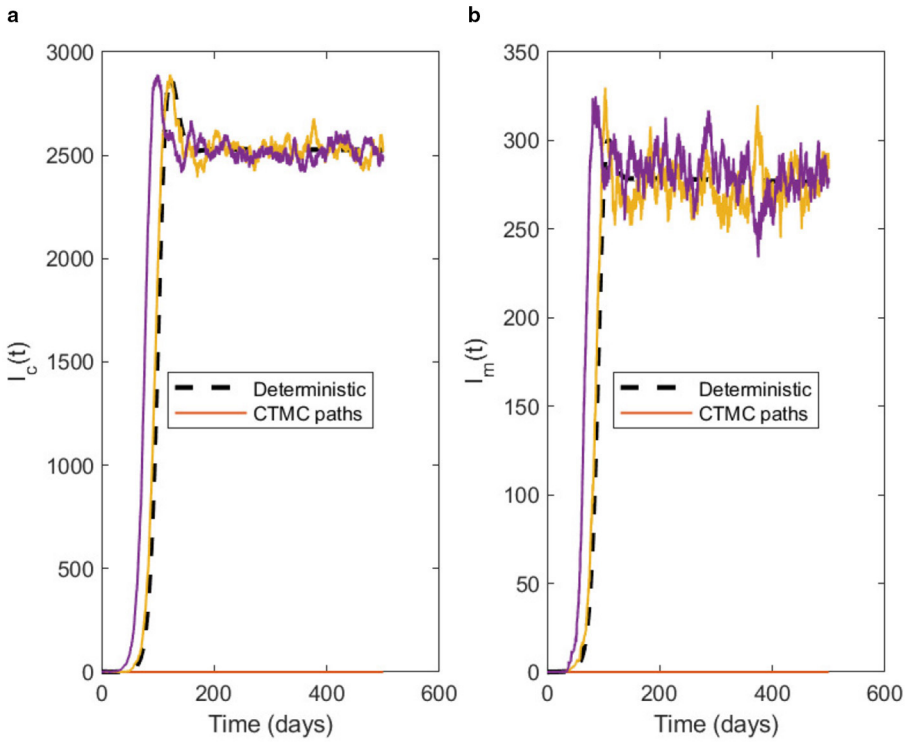

FIGURE 4
Representative CTMC stochastic realizations (solid curves) compared with the deterministic model outputs (dashed curves) for **(a)** infectious immunocompetent humans I_c and **(b)** infectious immunocompromised humans I_m. Solid curves represent multiple stochastic realizations of the CTMC model, included to illustrate demographic randomness and variability in outbreak trajectories, while dashed curves denote the corresponding deterministic solution.

the small extinction probabilities P_0 for I_l and G_p. The figure therefore supports the conclusion that, given the parameter values considered, giardiasis is unlikely to go extinct once established in the livestock or environmental classes.

Overall, the extinction analysis and the sample-path behavior demonstrate that the giardiasis infection is more likely to fade out when emerging from human infectious classes, especially the immunocompetent group. In contrast, outbreaks originating from lambs or the environment exhibit a high probability of persistence, highlighting the significant epidemiological role of these two reservoirs as already implied by the environmental transmission terms and shedding rates introduced in Section 2.

4.3 Sensitivity of human and lamb shedding rates on P_0

While Section 4.2 characterizes the baseline probability of giardiasis extinction from different initiating infectious classes, it is equally important to assess how this probability changes under perturbations of key transmission parameters. In giardiasis, the shedding of Giardia cysts by infected hosts and their persistence in the The environment plays a dominant role in sustaining transmission chains. Even modest changes in shedding intensity or environmental contamination may therefore substantially alter the likelihood of disease fade-out or persistence.

In this subsection, we investigate the sensitivity of the extinction probability P_0 to variations in the cyst shedding rates ϕ_c, ϕ_m, and ϕ_ℓ, corresponding to immunocompetent humans, immunocompromised humans, and lambs, respectively. We also examine the combined effect of simultaneously varying ϕ_c and ϕ_m. The results are summarized in Tables 5–8 and visualized in Figures 10, 11.

The analysis is conducted within the four-type branching process approximation described in Section 3.2. Recall that the infectious entities are classified as Type 1: I_c, Type 2: I_m, Type 3: I_l, and Type 4: G_p. The branching process is fully specified by the 4×4 mean offspring matrix $M = (m_{ij})$, where m_{ij} denotes the expected number of type-j offspring generated by a single type-i entity during its infectious or viable lifetime.

Under the assumption that susceptible populations remain close to their disease-free equilibrium values, the offspring distributions are Poisson and the probability-generating functions take the form

$$G_i(\mathbf{s}) = \exp\left(\sum_{j=1}^{4} m_{ij}(s_j - 1)\right), \qquad i = 1, \ldots, 4.$$

Let $\mathbf{q} = (q_1, q_2, q_3, q_4)$ denote the extinction probability vector, where q_i is the probability that giardiasis eventually dies out when initiated by a single type-i entity. Then $\mathbf{q}$ is the minimal non–negative solution of the fixed–point system

$$\mathbf{q} = \mathbf{G}(\mathbf{q}).$$

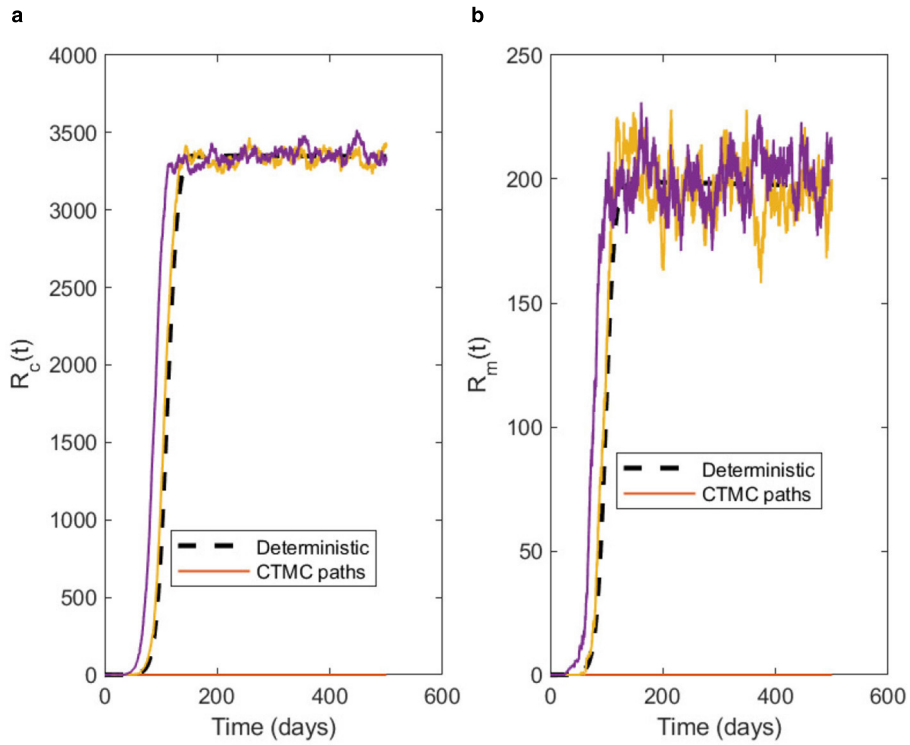

FIGURE 5
Illustrative CTMC stochastic realizations (solid curves) together with the corresponding deterministic model trajectories (dashed curves) for **(a)** recovered immunocompetent humans R_c and **(b)** recovered immunocompromised humans R_m. Solid curves represent multiple stochastic realizations of the CTMC model, included to illustrate demographic randomness and variability in outbreak trajectories, while dashed curves denote the corresponding deterministic solution.

For an initial condition $\mathbf{x}_0 = (x_1, x_2, x_3, x_4)$, the extinction probability is

$$P_0(\mathbf{x}_0) = \prod_{i=1}^{4} q_i^{x_i}.$$

This formula forms the basis for all entries reported in Tables 5–8.

Next, we carry out the parameter perturbation procedure and let $\phi^{(0)}$ denote the baseline value of a shedding parameter listed in Table 3. For a given percentage change $\delta \in [-90\%, 90\%]$, we define the perturbed value as

$$\phi = (1 + \delta)\,\phi^{(0)}.$$

For each perturbed parameter set, the following steps are performed:

1. The disease-free equilibrium susceptible levels are kept fixed.
2. The mean offspring matrix M is reconstructed using the modified shedding rate.
3. The fixed–point equation $\mathbf{q} = \mathbf{G}(\mathbf{q})$ is solved numerically.
4. The extinction probabilities P_0 are computed using the product formula above for each outbreak initiation scenario.

This procedure is repeated independently for variations in ϕ_c, ϕ_m, ϕ_l, and for the joint variation of ϕ_c and ϕ_m.

Tables 5–7 report the extinction probabilities when ϕ_c, ϕ_m, and ϕ_ℓ They are varied individually. A clear monotonic relationship is observed: increasing any shedding rate leads to a systematic decrease in P_0, reflecting the enhanced probability that an infectious individual generates a sufficiently large transmission chain. Conversely, reducing shedding substantially increases the likelihood of extinction, even when the deterministic reproduction number exceeds unity. The sensitivity is most pronounced for ϕ_ℓ, indicating that lamb–derived cyst shedding contributes disproportionately to early amplification of giardiasis. This is consistent with the relatively high cyst production rate of infected lambs and the additional transmission pathway through environmental contamination.

Table 8 and Figure 11 examine the simultaneous perturbation of ϕ_c and ϕ_m. Joint increases in human shedding rates have a synergistic effect, producing a sharper decline in extinction probability than altering either parameter alone. This highlights the role of heterogeneous human infectiousness in sustaining giardiasis, particularly in settings with a high prevalence of immunocompromised individuals.

Figures 10,11 illustrate the sensitivity patterns reported in Tables 5–8. In Figure 10, the extinction probability P_0 is plotted against percentage changes in ϕ_c and ϕ_m, while Figure 11 displays the corresponding trends for ϕ_l and for the combined variation of ϕ_c and ϕ_m. Across all scenarios, the graphical results reinforce the tabulated findings and clearly demonstrate the nonlinear impact of shedding parameters on early extinction dynamics.

These results underscore the importance of interventions that reduce cyst shedding or environmental contamination,

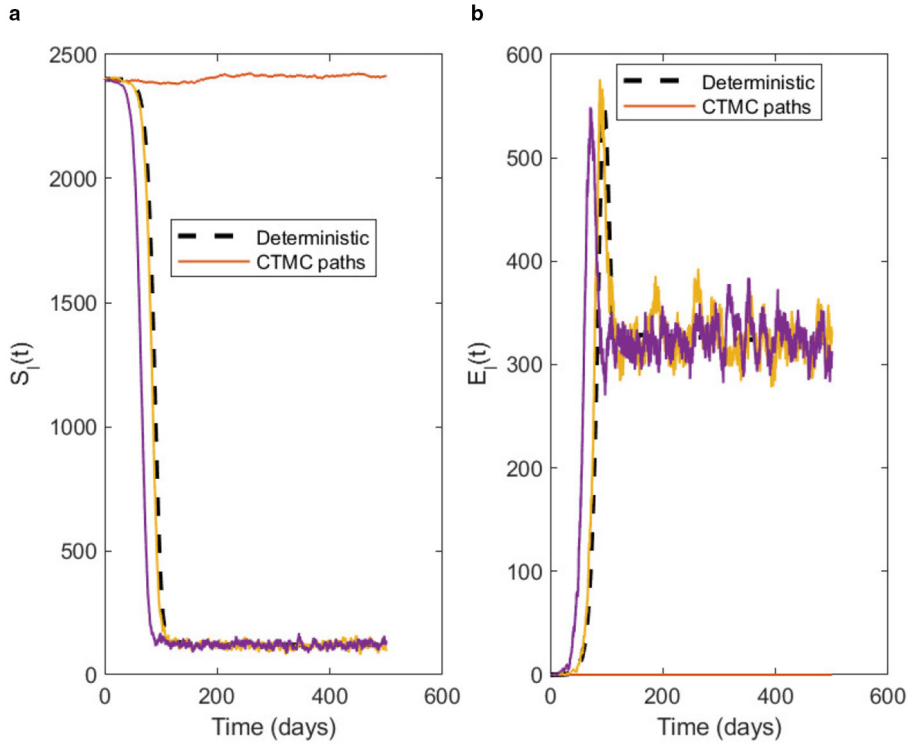

FIGURE 6
Representative stochastic trajectories generated by the CTMC framework (solid curves) compared with the associated deterministic solutions (dashed curves) for **(a)** susceptible lambs S_l and **(b)** exposed lambs E_l. Solid curves represent multiple stochastic realizations of the CTMC model, included to illustrate demographic randomness and variability in outbreak trajectories, while dashed curves denote the corresponding deterministic solution.

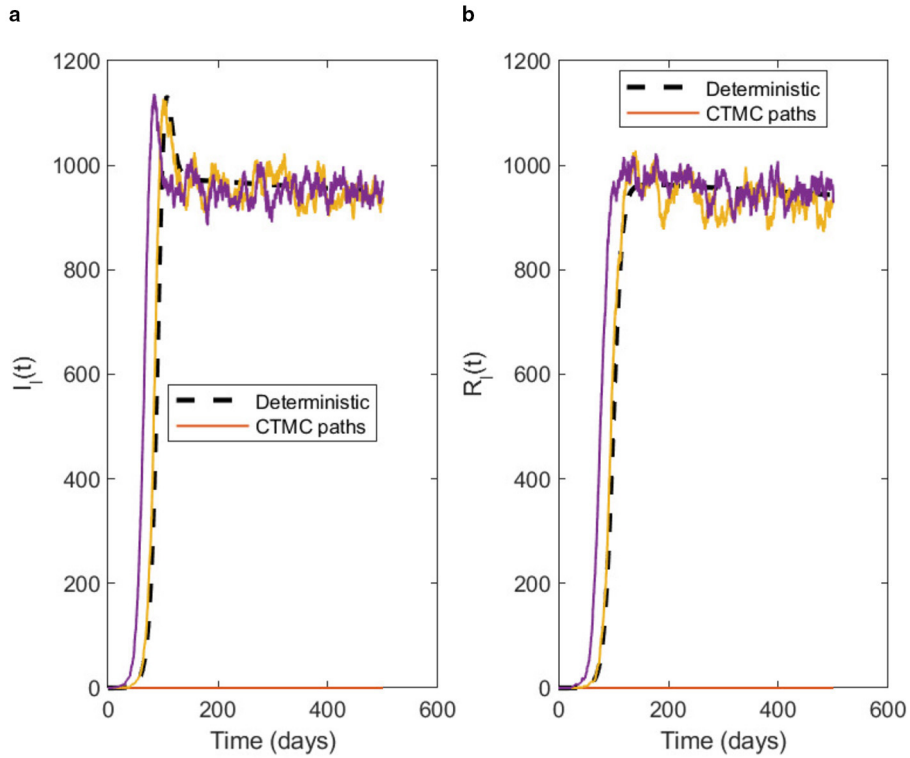

FIGURE 7
Sample CTMC-based stochastic realizations (solid curves) alongside the corresponding deterministic model trajectories (dashed curves) for **(a)** infectious lambs I_l and **(b)** recovered lambs R_l. Solid curves represent multiple stochastic realizations of the CTMC model, included to illustrate demographic randomness and variability in outbreak trajectories, while dashed curves denote the corresponding deterministic solution.

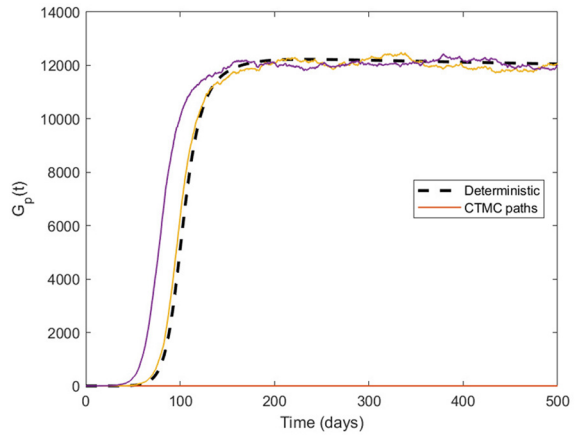

FIGURE 8
Representative CTMC stochastic realizations (solid curves) compared with the associated deterministic trajectory (dashed curve) for the environmental Giardia cyst concentration G_p. Solid curves represent multiple stochastic realizations of the CTMC model, included to illustrate demographic randomness and variability in outbreak trajectories, while dashed curves denote the corresponding deterministic solution.

such as rapid treatment, improved hygiene, and wastewater management. From a stochastic perspective, even moderate reductions in shedding can dramatically increase the probability of giardiasis extinction, emphasizing that control strategies need not only reduce $\mathcal{R}_0$ but also enhance the likelihood of early stochastic fade–out.

4.4 Distribution of the extinction time of giardiasis

In addition to evaluating the probability of disease extinction, it is informative to examine the distribution of the finite time to extinction $\mathcal{T}$ under the CTMC formulation. For each of the four single-introduction scenarios considered—namely $I_c(0) = 1$, $I_m(0) = 1$, $I_\ell(0) = 1$, and $G_p(0) = 1$, we generated a large number of sample paths of the stochastic system and recorded the time at which all infectious and exposed states reached zero. This procedure follows the same philosophy used in Luhanda et al. [31], but adapted to the reduced set of introduction scenarios relevant to giardiasis.

For each scenario, the empirical extinction probability $\widehat{P}_0$ was computed as the proportion of simulated paths that eventually died out before the terminal time horizon. Conditional on extinction, the extinction times were summarized by their empirical distribution and mean extinction time $\widehat{T}$. The resulting histograms, displayed in Figure 12, show markedly different patterns depending on the class in which the infection is introduced.

Consistent with the branching-process analysis in Section 4.1, the scenarios initiated by infected lambs (I_l) and environmental cysts (G_p) exhibit the lowest extinction probabilities. Their extinction-time distributions are right-skewed with comparatively short means, reflecting rapid early transmission followed by eventual decay once stochastic fade-out occurs. In contrast, introduction through infectious humans (I_c or I_m) leads to substantially higher probability of extinction and longer average extinction times. This is consistent with the weaker contribution of human-to-environment and human-to-human transmission pathways compared with the lamb-driven environmental amplification loop identified in earlier sections.

TABLE 4 Extinction probabilities P_0 (branching process) and numerical approximations P_a from CTMC simulations for single introductions in (I_c, I_m, I_ℓ, G_p).

x_1	x_2	x_3	x_4	P_0	P_a
1	0	0	0	0.568512	0.56839
0	1	0	0	0.510405	0.50811
0	0	1	0	8.91332×10^{-5}	0.0001
0	0	0	1	0.00414366	0.0039
1	1	1	1	1.07171×10^{-7}	0

The quantitative summaries of extinction probability and conditional mean extinction time for each introduction scenario are provided in Table 9. Together, Table 9 and Figure 12 reinforce the conclusion that giardiasis is far more persistent when initiated from an infected lamb or from cysts already present in the environment, whereas human-initiated infections have a significantly higher likelihood of dying out, albeit over a longer time frame. These findings complement the sensitivity results of Section 4.3 and highlight the dominant role of the animal-environment transmission pathway in shaping giardiasis persistence.

5 Conclusion

In this work, we developed and analyzed a deterministic and stochastic framework for the transmission dynamics of giardiasis in a coupled human-animal-environment system. The formulation incorporates heterogeneous human susceptibility, explicitly distinguishing immunocompetent and immunocompromised hosts, as well as a lamb population and an environmental reservoir of viable cysts. This structure enabled us to capture the important pathways through which infection may be established, persist, or die out.

The deterministic subsystem was shown to admit a unique disease-free equilibrium, and the associated basic reproduction number $\mathcal{R}_0$ was derived. Sensitivity analysis of $\mathcal{R}_0$ revealed that parameters linked to cyst shedding particularly ϕ_c (immunocompetent humans), ϕ_m (immunocompromised humans), and ϕ_l (lambs) play dominant roles in determining whether giardiasis can invade a susceptible population. These findings are consistent with biological expectation, since cyst output governs the replenishment of the environmental reservoir that drives indirect transmission.

To quantify early-outbreak behavior, a multitype branching process approximation was constructed. This approximation allowed the computation of the extinction probabilities P_0 for several initial infection scenarios. The baseline extinction probabilities in Table 4 indicate that introduction through

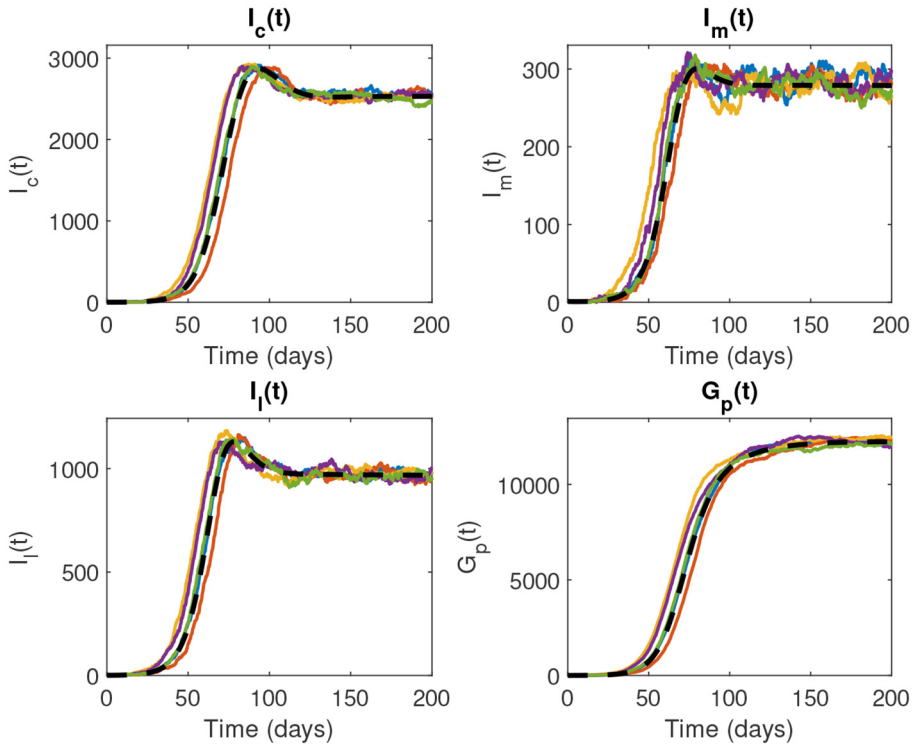

FIGURE 9
CTMC sample paths (colored curves) and deterministic trajectories (black dashed curves) for the infectious classes (I_c, I_m, I_ℓ) and the environmental cyst concentration G_p. The stochastic trajectories exhibit early fluctuations before stabilizing near the deterministic solution.

TABLE 5 Impact of varying ϕ_c on P_0.

x_1	x_2	x_3	x_4	$P_0(-90\%)$	P_0	$P_0(+90\%)$
1	0	0	0	0.8844	0.5502	0.3756
0	1	0	0	0.6465	0.5831	0.58
0	0	1	0	0.00142	0.0002817	0.0002584
0	0	0	1	0.2144	0.01419	0.003514
1	1	1	1	0.0001741	1.282e-06	1.978e-07

TABLE 6 Impact of varying ϕ_m on P_0.

x_1	x_2	x_3	x_4	$P_0(-90\%)$	P_0	$P_0(+90\%)$
1	0	0	0	0.5822	0.5502	0.5335
0	1	0	0	0.9438	0.5831	0.3763
0	0	1	0	0.0003059	0.0002817	0.0002735
0	0	0	1	0.02442	0.01419	0.01053
1	1	1	1	4.105e-06	1.282e-06	5.781e-07

TABLE 7 Impact of varying ϕ_l on P_0.

x_1	x_2	x_3	x_4	$P_0(-90\%)$	P_0	$P_0(+90\%)$
1	0	0	0	0.5508	0.5502	0.5502
0	1	0	0	0.5838	0.5831	0.5831
0	0	1	0	0.3972	0.0002817	2.178e-07
0	0	0	1	0.01629	0.01419	0.01419
1	1	1	1	0.002081	1.282e-06	9.914e-10

TABLE 8 Impact of varying ϕ_c and ϕ_m on P_0.

x_1	x_2	x_3	x_4	$P_0(-90\%)$	P_0	$P_0(+90\%)$
1	0	0	0	0.9622	0.5502	0.3658
0	1	0	0	0.9718	0.5831	0.3737
0	0	1	0	0.01676	0.0002817	0.0002568
0	0	0	1	0.5197	0.01419	0.002758
1	1	1	1	0.008142	1.282e-06	9.684e-08

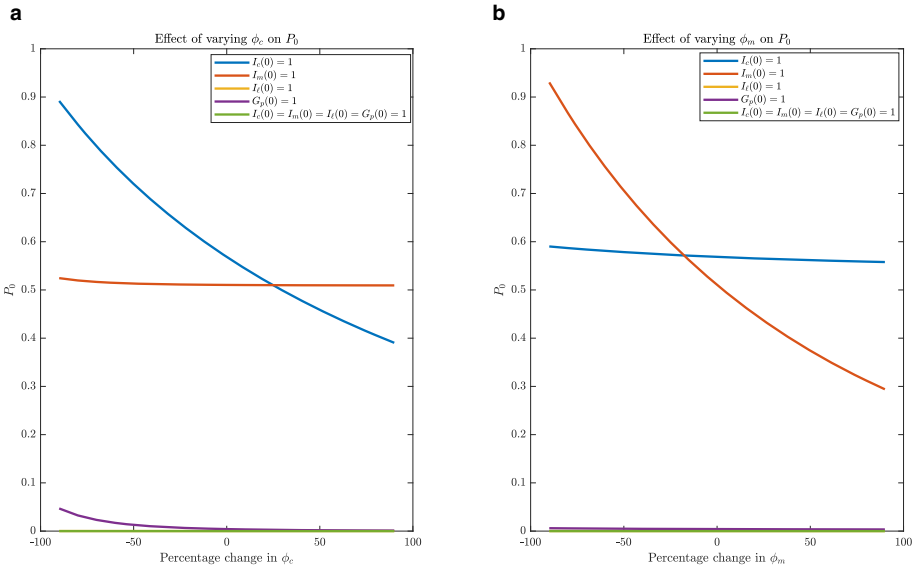

FIGURE 10
Impact of varying human shedding rates of *Giardia* cysts on the extinction probability P_0. Panels **(a)** and **(b)** show the effect of changing the shedding rate by infectious immunocompetent humans ϕ_c and infectious immunocompromised humans ϕ_m, respectively. In each panel, the shedding rate is varied by ±90% from its baseline value in Table 3, while all other parameters are held fixed. The corresponding extinction probabilities P_0 for the introduction scenarios (x_1, x_2, x_3, x_4) in Table 4 are reported in Tables 5, 6. Steeper slopes indicate greater sensitivity of P_0 to perturbations in the shedding rate, whereas flatter curves indicate weaker sensitivity. The legend entries match the four introduction scenarios listed in Table 4.

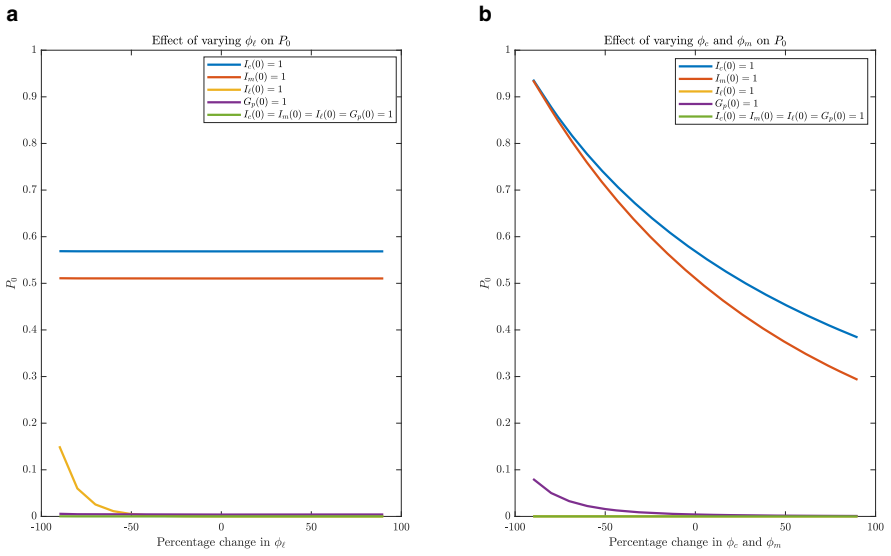

FIGURE 11
Impact of varying lamb and human shedding rates of *Giardia* cysts on the extinction probability P_0. Panel **(a)** shows the effect of perturbing the lamb shedding rate ϕ_l by ±90% from its baseline value in Table 3, with all other parameters fixed; the corresponding extinction probabilities P_0 for the introduction scenarios (x_1, x_2, x_3, x_4) are summarized in Table 7. Panel **(b)** illustrates the effect of changing the human shedding rates ϕ_c and ϕ_m simultaneously by ±90% from their baseline values, with extinction probabilities reported in Table 8. As in Figure 10, steeper slopes indicate higher sensitivity of P_0 to shedding-rate perturbations, while shallower slopes indicate lower sensitivity. The legend entries correspond to the four introduction scenarios described in Table 3.

immunocompetent or immunocompromised infectious humans has a significantly lower chance of immediate fade-out compared with introduction via lambs or cysts. Moreover, the shedding-sensitivity experiments (Tables 5–8) show that P_0 decreases rapidly as the shedding rates increase, emphasizing that environmental contamination is a key driver of persistence.

TABLE 9 Estimated extinction probability $\hat{P}_0$ and mean extinction time $\hat{T}$ (in days) for the CTMC stochastic model under four single-introduction scenarios.

Group initiating the disease	$\hat{P}_0$	$\hat{T}$ (days)
I_c	0.788	11.94
I_m	0.629	12.45
I_l	0.143	4.59
G_p	0.382	8.68

Each scenario corresponds to the introduction of one infectious host or a single viable cyst into a disease-free population. The estimates are obtained from N_{path} Monte Carlo sample paths simulated up to $T_{\max}$.

Complementing the branching-process calculations, a continuous-time Markov chain (CTMC) was employed to estimate the distribution of extinction times for the same introduction scenarios. The results (Table 9 and Figure 12) reveal that outbreaks initiated by infectious humans tend to persist longer than those initiated by lambs or cysts, even when eventual extinction is likely. This highlights an asymmetry between invasion probability and outbreak duration: a scenario with moderate extinction probability may still result in prolonged transmission before extinction occurs. The CTMC simulations therefore provide an additional layer of insight that cannot be extracted from deterministic analysis or branching-process theory alone.

Overall, the combined analytical and numerical results demonstrate that controlling cyst contamination and reducing shedding from infected hosts are crucial for preventing sustained transmission. Interventions such as improved sanitation, early diagnosis and treatment of human cases particularly among immunocompromised individuals–and targeted control of infection in lambs may substantially decrease both the probability

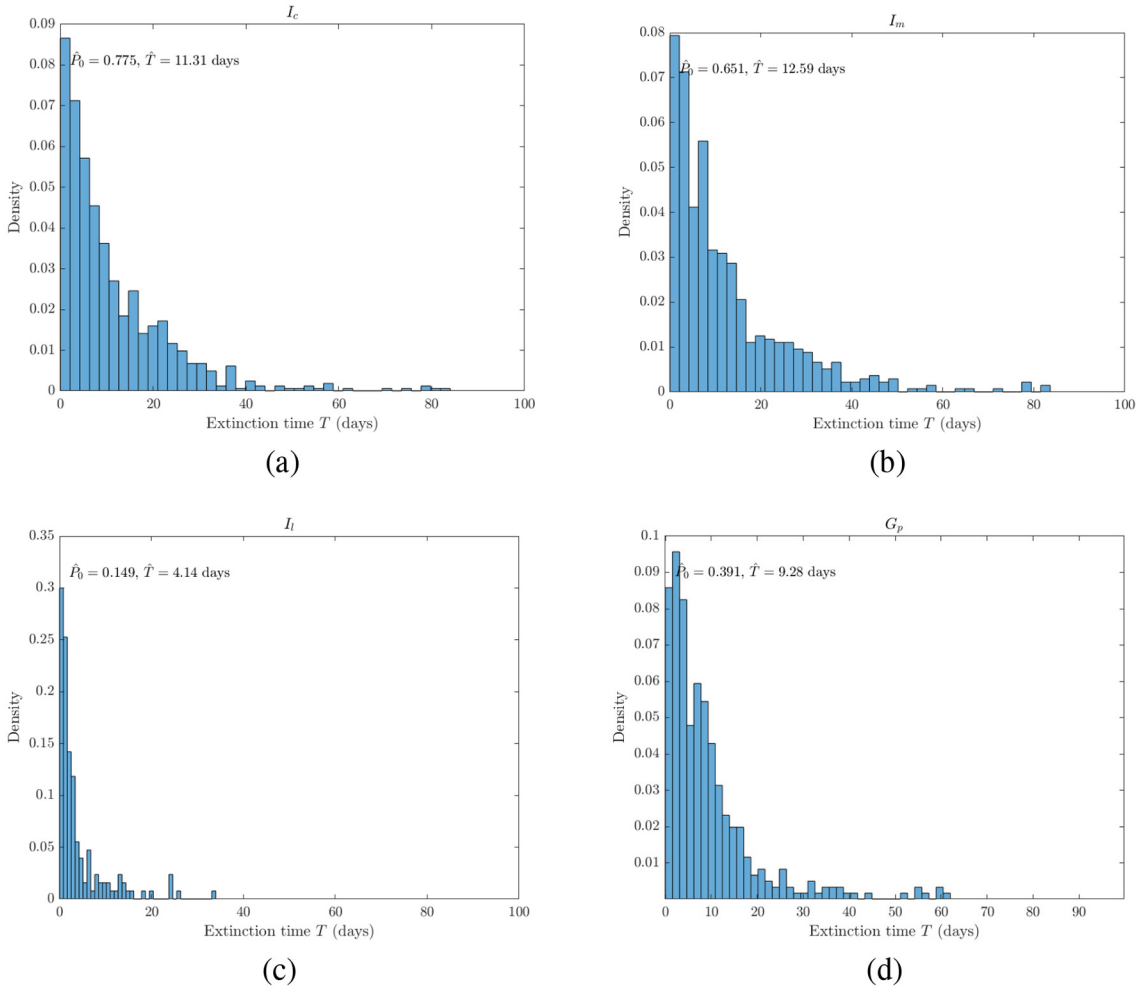

FIGURE 12
Distribution of extinction times obtained from CTMC simulations. **(a)** Histogram of extinction times for infectious immunocompetent humans I_c with $\beta h = 0.775$ $\beta h = 0.775$ and mean extinction time $T = 11.31$ days. **(b)** Histogram for infectious immunocompromised humans I_m with $\beta h = 0.651$ and mean $T = 12.59$ days. **(c)** Histogram for infectious lambs I_l with $\beta h = 0.149$ and mean $T = 4.14$. **(d)** Histogram for environmental cyst concentration G_p with $\beta h = 0.391$ and mean $T = 9.28$ days. All distributions exhibit right-skewed extinction-time profiles.

of invasion and the expected duration of outbreaks. Future extensions may incorporate seasonality, spatial heterogeneity, or host behavioral differences to furnish a more comprehensive understanding of the conditions promoting giardiasis persistence in mixed human-animal communities.

Data availability statement

The original contributions presented in the study are included in the article/supplementary material, further inquiries can be directed to the corresponding author.

Author contributions

CA: Conceptualization, Writing – original draft, Formal analysis. IO: Visualization, Formal analysis, Writing – review & editing, Validation, Supervision, Conceptualization, Writing – original draft.

Funding

The author(s) declared that financial support was not received for this work and/or its publication.

Conflict of interest

The author(s) declared that this work was conducted in the absence of any commercial or financial relationships that could be construed as a potential conflict of interest.

Generative AI statement

The author(s) declared that generative AI was not used in the creation of this manuscript.

Any alternative text (alt text) provided alongside figures in this article has been generated by Frontiers with the support of artificial intelligence and reasonable efforts have been made to ensure accuracy, including review by the authors wherever possible. If you identify any issues, please contact us.

Publisher's note

References

1. World Health Organization. *Giardiasis*. (2024). WHO Fact Sheets. Available online at: https://www.who.int/news-room/fact-sheets (Accessed October 31, 2024).

2. World Health Organization. *Giardiasis-Fact Sheet*. Geneva: World Health Organization (2023). Available online at: https://www.who.int/news-room/fact-sheets/detail/giardiasis (Accessed March 28, 2023).

3. World Health Organization. *Giardiasis: A Neglected Disease*. (2004). Available online at: https://www.who.int/news-room/fact-sheets/detail/giardiasis (Accessed January 20, 2025).

4. Feng Y, Xiao L. Zoonotic potential and molecular epidemiology of *Giardia* species and giardiasis. *Clin Microbiol Rev*. (2011) 24:110–40. doi: 10.1128/CMR.00033-10

5. Cotton JA, Beatty JK, Buret AG. Host parasite interactions and pathophysiology in *Giardia* infections. *Int J Parasitol*. (2011) 41:925–33. doi: 10.1016/j.ijpara.2011.05.002

6. Vivancos V, González-Alvarez I, Bermejo M, Gonzalez-Alvarez M. Giardiasis: characteristics, pathogenesis and new insights about treatment. *Curr Top Med Chem*. (2018) 18:1287–303. doi: 10.2174/1568026618666181002095314

7. Liana YA, Chuma FM. Mathematical modeling of giardiasis transmission dynamics with control strategies in the presence of carriers. *J Appl Math*. (2023) 2023:1562207. doi: 10.1155/2023/1562207

8. Edward S, Shaban N. Deterministic compartmental model for optimal control strategies of Giardiasis infection with saturating incidence and environmental dynamics. *Healthc Anal*. (2025) 7:100383. doi: 10.1016/j.health.2025.100383

9. Hamilton KA, Waso M, Reyneke B, Saeidi N, Levine A, Lalancette C, et al. Cryptosporidium and Giardia in wastewater and surface water environments. *J Environ Qual* (2018) 47:1006–23. doi: 10.2134/jeq2018.04.0132

10. Dixon B, Parrington L, Cook A, Pintar K, Pollari F, Kelton D, et al. The potential for zoonotic transmission of Giardia duodenalis and Cryptosporidium spp, from beef and dairy cattle in Ontario, Canada. *Vet Parasitol*. (2011) 175:20–6. doi: 10.1016/j.vetpar.2010.09.032

11. Lalle M, Hanevik K. Treatment-refractory giardiasis: challenges and solutions. *Infect Drug Resist*. (2018) 11:1921–33. doi: 10.2147/IDR.S141468

12. Robertson L, Forberg T, Gjerde B. Giardia cysts in sewage influent in Bergen, Norway 15-23 months after an extensive waterborne outbreak of giardiasis. *J Appl Microbiol*. (2008) 104:1147–52. doi: 10.1111/j.1365-2672.2007.03630.x

13. Das P, Das S, Upadhyay RK, Das P. Optimal treatment strategies for delayed cancer-immune system with multiple therapeutic approach. *Chaos Solitons Fractals*. (2020) 136:109806. doi: 10.1016/j.chaos.2020.109806

14. Das P, Das S, Das P, Rihan FA, Uzuntarla M, Ghosh D. Optimal control strategy for cancer remission using combinatorial therapy: a mathematical model-based approach. *Chaos Solitons Fractals*. (2021) 145:110789. doi: 10.1016/j.chaos.2021.110789

15. Luhanda F, Mayengo M, Irunde J, Chirove F. Transmission dynamics of cryptosporidiosis in humans and cattle: a CTMC stochastic model integrating the role of human immune status. *Franklin Open*. (2025) 11:100258. doi: 10.1016/j.fraope.2025.100258

16. Charles M, Mfinanga SG, Lyakurwa G, Torres DF, Masanja VG. Evaluating the effectiveness of Stochastic CTMC and deterministic models in correlating rabies persistence in human and dog populations. *Franklin Open*. (2025) 13:100397. doi: 10.1016/j.fraope.2025.100397

17. Tilahun GT, Woldegerima WA, Wondifraw A. Stochastic and deterministic mathematical model of cholera disease dynamics with direct transmission. *Adv Diff Equ*. (2020) 2020:670. doi: 10.1186/s13662-020-03130-w

18. Hale JK. *Ordinary Differential Equations*. North Chelmsford, MA: Courier Corporation (2009).

19. Diekmann O, Heesterbeek JAP, Metz JAJ. On the definition and the computation of the basic reproduction ratio R 0 in models for infectious diseases in heterogeneous populations. *J Math Biol*. (1990) 28:365–82. doi: 10.1007/BF00178324

20. Van den Driessche P, Watmough J. Reproduction numbers and sub-threshold endemic equilibria for compartmental models of disease transmission. *Math Biosci*. (2002) 180:29–48. doi: 10.1016/S0025-5564(02)00108-6

21. Kamgang JC, Sallet G. Computation of threshold conditions for epidemiological models and global stability of the disease-free equilibrium (DFE). *Math Biosci*. (2008) 213:1–12. doi: 10.1016/j.mbs.2008.02.005

22. Mgandu FA, Mirau S, Nyerere N, Mbega E, Chirove F. Mathematical model to assess the impacts of aflatoxin contamination in crops, livestock and humans. *Sci Afr*. (2024) 23:e01980. doi: 10.1016/j.sciaf.2023.e01980

23. Stephano MA, Irunde JI, Mayengo MM, Kuznetsov D. The significance of stochastic CTMC over deterministic model in understanding the dynamics of lymphatic filariasis with asymptomatic carriers. *J Appl Math*. (2024) 2024:2130429. doi: 10.1155/2024/2130429

24. La Salle JP. The stability of dynamical systems. *SIAM*. (1976) 25:57–76. doi: 10.1137/1.9781611970432

25. Allen LJ. An introduction to stochastic epidemic models. In: *Mathematical Epidemiology*. Cham: Springer (2008). p. 81–130. doi: 10.1007/978-3-540-78911-6_3

26. Maliyoni M. Probability of disease extinction or outbreak in a stochastic epidemic model for west Nile virus dynamics in birds. *Acta Biotheor*. (2021) 69:91–116. doi: 10.1007/s10441-020-09391-y

27. Lloyd AL, Zhang J, Root AM. Stochasticity and heterogeneity in host-vector models. *J R Soc Interface*. (2007) 4:851–63. doi: 10.1098/rsif.2007.1064

28. Lahodny GE Jr, Allen LJ. Probability of a disease outbreak in stochastic multipatch epidemic models. *Bull Math Biol*. (2013) 75:1157–80. doi: 10.1007/s11538-013-9848-z

29. Allen LJ. *An Introduction to Stochastic Processes with Applications to Biology*. Boca Raton, FL: CRC Press (2010). doi: 10.1201/b12537

30. Lahodny G Jr, Gautam R, Ivanek R. Estimating the probability of an extinction or major outbreak for an environmentally transmitted infectious disease. *J Biol Dyn*. (2015) 9:128–55. doi: 10.1080/17513758.2014.954763

31. Luhanda F, Mayengo MM, Irunde JI, Chirove F. The role of human immune status on the transmission dynamics of cryptosporidiosis in humans and cattle. *Model Earth Syst Environ*. (2024) 10:7251–79. doi: 10.1007/s40808-024-02146-5

32. Allen LJ, van den Driessche P. Relations between deterministic and stochastic thresholds for disease extinction in continuous-and discrete-time infectious disease models. *Math Biosci*. (2013) 243:99–108. doi: 10.1016/j.mbs.2013.02.006

33. Mode CJ. *Multitype Branching Processes: Theory and Applications*. New York, NY: American Elsevier Publishing Company (1971).

34. Bastiaansen R, Chirilus-Bruckner M, Doelman A. Pulse solutions for an extended Klausmeier model with spatially varying coefficients. *SIAM J Appl Dyn Syst*. (2020) 19:1–57. doi: 10.1137/19M1255665

35. Mpeshe S, Nyerere N. A human-animal model of giardiasis infection in contaminated environment. *Int J Adv Appl Mathem Mech*. (2021) 8:37–47.

36. Conners EE. Giardiasis outbreaks—United States, 2012-2017. *MMWR Morb Mortal Wkly Rep*. (2021) 70:304–7. doi: 10.15585/mmwr.mm7009a2

37. Osman S, Togbenon HA, Otoo D. Modelling the dynamics of campylobacteriosis using nonstandard finite difference approach with optimal control. *Comput Math Methods Med*. (2020) 8843299. doi: 10.1155/2020/8843299

38. Kitowska W, Sadkowska-Todys M. Giardiasis (lambliasis) in Poland in 2020. *Przegląd Epidemiologiczny-Epidemiol Rev*. (2023) 76:616–25. doi: 10.32394/pe.76.56